# REACTOR CAVITY COOLING SYSTEM HEAT REMOVAL ANALYSIS FOR A HIGH TEMPERATURE GAS COOLED REACTOR

By

HONG-CHAN WEI

A THESIS PRESENTED TO THE GRADUATE SCHOOL
OF THE UNIVERSITY OF FLORIDA IN PARTIAL FULFILLMENT
OF THE REQUIREMENTS FOR THE DEGREE OF
MASTER OF SCIENCE

UNIVERSITY OF FLORIDA

2009

To my Father, Hen-Po Wei

ACKNOWLEDGMENTS

I would like to thank Dr. Samim Anghaie for being my advisor, Dr. Edward Dugan and Dr. Glenn Sjoden for being members of my supervisory committee. I would like to particularly express my sincere gratitude to Dr. Edward Dugan who succeeded Dr. Samim Anghaie as my new advisor and provided his patience and support.

I would like to acknowledge Dr. Anne Charmeau and Bobby Ahmed for their patience and assistance in teaching me to be familiar with FLUENT. I would like to thank Michael Rose for his patience of improving my English speaking.

Innovative Nuclear Space Power and Propulsion Institute (INSPI) at the University of Florida provided support for this research.

I would like to thank my parents for their endless love, support and encouragement, and my friends for encouraging me during my worst period.

TABLE OF CONTENTS

LIST OF TABLES

LIST OF FIGURES

Abstract of Thesis Presented to the Graduate School
of the University of Florida in Partial Fulfillment of the
Requirements for the Degree of Master of Science

# REACTOR CAVITY COOLING SYSTEM HEAT REMOVAL ANALYSIS FOR A HIGH TEMPERATURE GAS COOLED REACTOR

By

Hong-Chan Wei

August 2009

Chair: Edward Dugan
Major: Nuclear Engineering Sciences

The HTR-10 is a small high temperature gas-cooled reactor. It is an experimental pebble-bed helium cooled reactor with a maximum power of 10 MW, constructed between 2000 and 2003 in China. The study focuses on the thermal-fluid analysis of the Reactor Cavity Cooling System (RCCS) with water flows up the pipes to cool the containment. Computational fluid dynamics (CFD) is used to study local heat transfer phenomena in the HTR-10 containment. Heat is transferred to the RCCS mainly via radiation, and to a lesser extent via natural convection. CFD allows for detailed modeling of both heat transfer modes. Sensitivity analyses on the computational grid and the physics models are performed to optimize the simulation. This leads to the use of the k-ω model for turbulence and Discrete Ordinates model for radiation. A 2D axisymmetric model is developed to simulate two scenarios from the HTR-10 benchmark exercises provided in the IAEA Coordinated Research Program (CRP-3). The first is a heat up experiment at a reactor power of 200 kW. The experiment simulates normal operation at low power and aims at verifying the RCCS heat removal capability under steady-state conditions. The second is a transient depressurized loss of heat sink accident. In this situation, the reactor is assumed to be running initially at full power, and then the temperature of the core barrel rises over the next 40 hours, peaks, and falls over the next 72 hours. Three fluids are modeled: the

helium inside the pressure vessel and outside the core vessel, air in the containment, and water in the RCCS. The boundary conditions are a temperature profile on the core barrel and adiabatic conditions on the containment walls. The simulations lead to safe values of temperature for all the reactor components; also, the computed temperatures compare well with previous simulations performed for the CRP-3.

# CHAPTER 1
# INTRODUCTION

## Introduction

Electricity demand has increased dramatically in past decades. Global Warming, green house gases, and the energy problems have also become the significant topics. Nuclear power seems to be the best solution for new energy supplies, because nuclear power is clear than fossil fuels. The pressurized water reactor (PWR) and the boiling water reactor (BWR) are two designs which are most used in nuclear power plants, especially the PWR. The PWR is a Generation II reactor that uses water under high pressure as the primary coolant to remove heat from nuclear fuel. Highly pressurized water is also used for moderating the neutron flux into the thermal energy region to maintain the nuclear reaction. Another nuclear reactor concept that has been developed since the 1950's is called the high temperature gas-cooled reactor (HTGR), which is also known as the Very High Temperature Reactor (VHTR). The temperature of the fuel in the HTGR is up to 1600℃, and the helium coolant outlet temperature is easily over 750℃ [1]. Based on this high temperature operation, the HTGR presents some benefits that are presented and discussed later. Although HTGRs can produce such high temperature, the study of the reactor reactivity is important, as well for maintaining reactor operation but not overheating. Therefore, studying reactor kinetics becomes a main issue in the nuclear power plant: controlling the reactivity in the reactor and controlling the heat flux and temperature. Especially important are temperatures, such as: those of the core vessel, the reflector, the pressure vessel, the reactor cavity cooling system (RCCS), and the concrete containment. In order to study the behavior of temperature, it is necessary to have an understanding of heat transfer, which can occur in primarily three ways: conduction, convection, and radiation. Heat in the reactor core is basically transferred to the RCCS through radiation because of the high temperature. Figure 1-1 illustrates

the location of the RCCS in the reactor. The RCCS utilizes water as the coolant to remove heat via the natural circulation of water. This research discusses the works of the RCCS.

## Why a High Temperature Gas-Cooled Reactor?

Both BWR and PWR designs are light water reactors (LWR). The LWR uses a steam turbine and has around 35% thermal efficiency. However, the thermal efficiency is not as high as HTGR which has been developed since 1950's. The current HTGR concept that is a Generation IV reactor and supported by the U.S. Department of Energy (DOE) is a graphite-moderated and helium gas-cooled reactor. The HTGR is attractive as one of the future energy options due to a number of advantages: the safety features, the ability of generating high temperature heat, a higher electricity efficiency, and the potential for hydrogen production and sea water desalination [2]. For example, the higher safety is due to its ability to use natural convection and radiation, and shutdown by itself because of the negative temperature reactivity coefficient [1]. Because the HTGR has become popular and significant, Russia, Germany, USA, South Africa, Japan and China are all working to develop their own HTGR designs. After 30 years of research, operating HTGRs or VHTRs included Fort St. Vrain in the USA and THTR-300 in Germany in the 1980's. Japan and China established their own HTGR models in 1998 and 2003, and they are the HTTR and HTR-10, respectively. Russia developed an HTGR in 1973 and the design is called VGM [3]. South Africa has a design of the HTGR called PBMR, constructed in 1999. Compared with conventional nuclear plants, the HTGR is a next generation nuclear plant (NGNP) due to several distinct advantages. First of all, the HTGR has a high thermal efficiency, up to 48% [3], which is significantly larger than for the BWR or PWR. Generally speaking, this high efficiency is higher than any traditional power plants. Additionally, the attractive ambrosia is its byproduct, hydrogen that is widely used in the world. Hydrogen can be utilized for several purposes, and the most important use is as the clean fuel. The main technology of getting

hydrogen in industry is through high temperature electrolysis. This thermal process of producing hydrogen can directly use heat provided by the HTGR. Moreover, nuclear power plants do less damage to the environment than traditional power plants. High burn-up and increased safety are other advantages of HTGR as well, so using nuclear power has more benefits than fossil fuel power plants.

## Thesis Objective

Heat generation rate depends on how effectively neutrons maintain the nuclear reaction. If the reactor is critical, it means the neutron's population remains constant. The proper amounts of neutrons balance the reaction in the reactor; therefore, the heat generation rate is steady, and the research starts from the steady state. A computational fluid dynamics (CFD) code was implemented to study the local heat removed by the RCCS and the ability to dissipated heat in the HTGR. FLUENT [4] is the CFD code utilized in this research to reproduce the benchmark problems of HTR-10, one of the current operating HTGR. The benchmark problems are also simulated for sensitivity analysis, which is useful for searching for the best or the optimized model. The temperature profiles in the benchmark problems obtained from the report TECDOC 1163 CRP-3 [1] are the references to be estimated in FLUENT. Hence, the exercises defined in this thesis are code-to-code benchmark problems, and the purpose of this research is to reproduce benchmark problems, perform sensitivity analysis, and compare data obtained from CRP-3 [1].

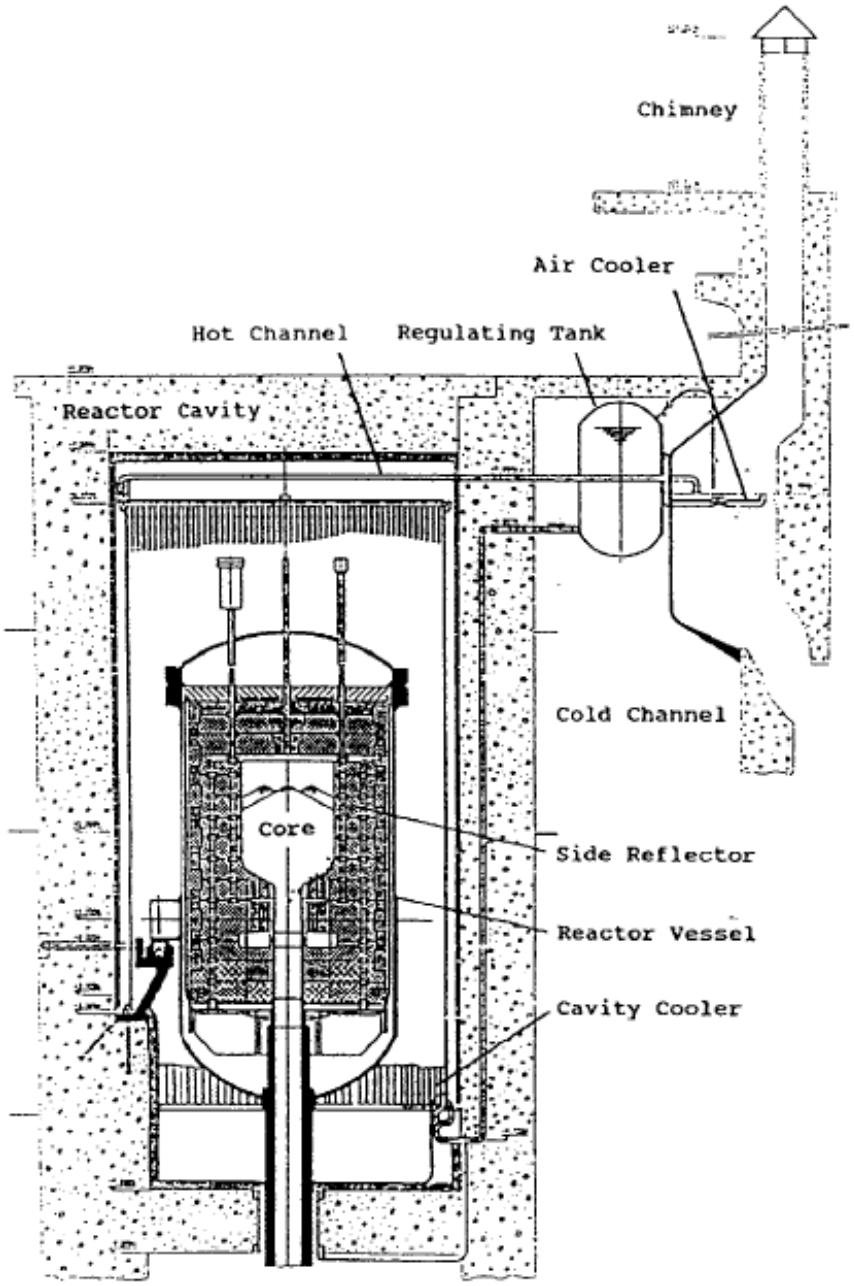


Figure 1-1. The physical constructions in the reactor include the RCCS, Pressure Vessel, the Core Vessel and chimney [5].

# CHAPTER 2
# HIGH TEMPERATURE GAS-COOLED REACTOR IN CHINA (HTR-10)

## Background

A small test HTGR in China called HTR-10 was built between 2000 to 2003 by Tsinghua University. HTR-10 is a pebble bed reactor with a full thermal power of 10 MW, and includes two passive decay heat removal systems, referred to as RCCS, with a total heat removal of 250 kW [1]. In the HTR-10, 27,500 TRISO particles, called pebbles, use uranium dioxide coated by graphite as the nuclear fuel; basically, U-235 is employed as the fissile material. Figure 2-1 displays the reactor core and the primary helium cooling system. Heat is generated from the nuclear fission process in fuel, and transferred to the helium coolant that is part of the primary cooling system connected to the heat exchanger. The gas duct was designed to transport hot helium and cold helium connecting the pressure vessel and the heat exchanger, where a gas turbine-steam turbine combine cycle was connected. Table 2-1 lists the primary system parameters of the HTR-10 design [1].

The HTGR has been researched and developed in China for nearly 50 years. Based on the experience of HTR-10, the Chinese have designed a new module called High Temperature Gas-Cooled Reactor-Pebble bed Module (HTR-PM) which is planned for construction in 2010 with a thermal power of 450MW [2].

## Benchmark Problems

Four benchmark problems are represented in the CRP-3 report [1], and are a heat-up experiment I, a loss of heat sink accident (LOHS), a heat-up experiment II, and a loss of cooling accident (LOCA). Problem 1 and 2 can be assumed as a group compared to problem 3 and 4. The only difference between the two groups is whether the thermal shielding panel is taken into account or not, which means problem 1 and 2 are the same as problem 3 and 4 without the

additional thermal shielding panel. In this thesis, the studies of the sensitivity analysis and local heat transfer rate are simulated depending on problem 1 and 2.

**Problem 1- Heatup Experiment**

This simulated benchmark problem is referred to as "Benchmark Problem 1" by Gao (1997) who described it as a heat up experiment [6]. The helium blower in the steam generator was assumed to be turned off, so there was no circulation of primary coolant. The water cooling wall was intact and functioning normally; hence, it is focused on the ability of the heat removed by the RCCS. Gao also describes the details of the benchmark problem: the reactor operates at 200 kW at 1.0 bar operating air pressure; for the water cooling system, its mass flow rate is 5.22 kg/s with an inlet temperature of 64.5℃ [6]. This simulation includes a temperature profile as the boundary condition on the surface of the core barrel (Figure 2-2): top, side, and bottom. The data of the temperature distribution are obtained from Gao's 1997 report [6], and the multiple temperature values on the top and bottom of the core vessel shown in Figure 2-2 results from the temperature changing with position on the top and bottom surfaces. In order to reproduce the heat generation rate as 200kW, the temperature profile is used as the boundary condition. Moreover, the concept of implementing the temperature profile as the boundary condition is used in the later simulations.

**Problem 2- Depressurized LOHS Accident**

This is the second HTR-10 benchmark exercise described by the TECDOC [1]: the reactor operates at the normal power of 10MW, and the cooling wall mass flow rate is 5.22 kg/s with the initial inlet temperature of 50.4℃. The temperature profile of the core barrel is a function of position and time, and the inlet water temperature is a function of time as well. Before starting the transient simulation, the steady state at normal power uses these two initial temperature distributions as the boundary condition. Figure 2-3 and Figure 2-4 show the initial temperature

profile of the core barrel for this benchmark problem. The LOHS benchmark problem also described that the reactor lost its primary helium coolant and the thermal power decreased to 224 kW; then the reactor shut down automatically and cooled by the RCCS.

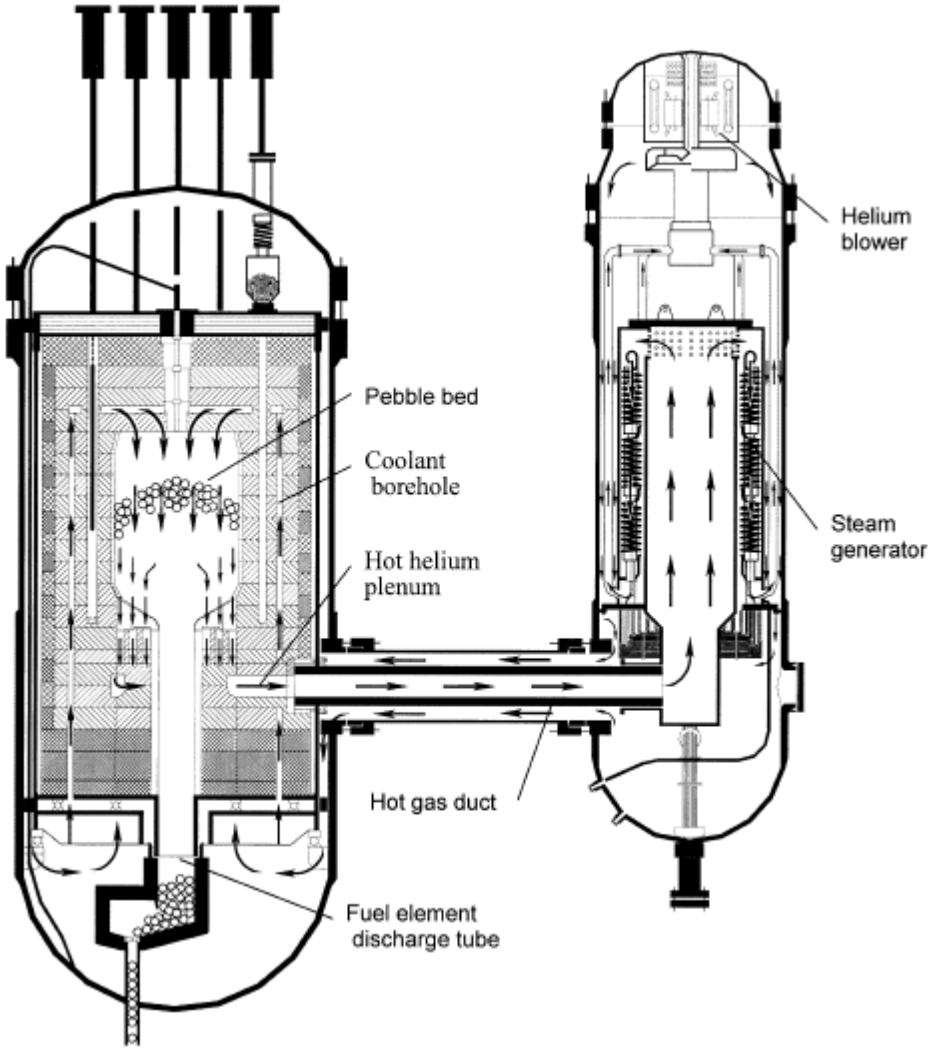


Figure 2-1. Reactor core, helium coolant and heat exchanger in the primary loop [7]

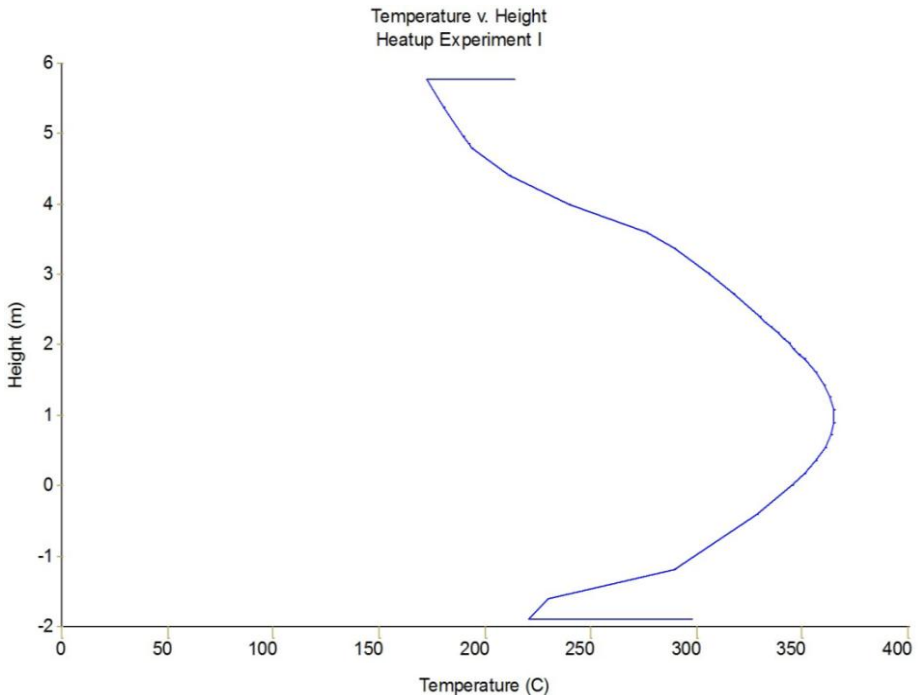

Figure 2-2. The temperature profile of the core barrel.

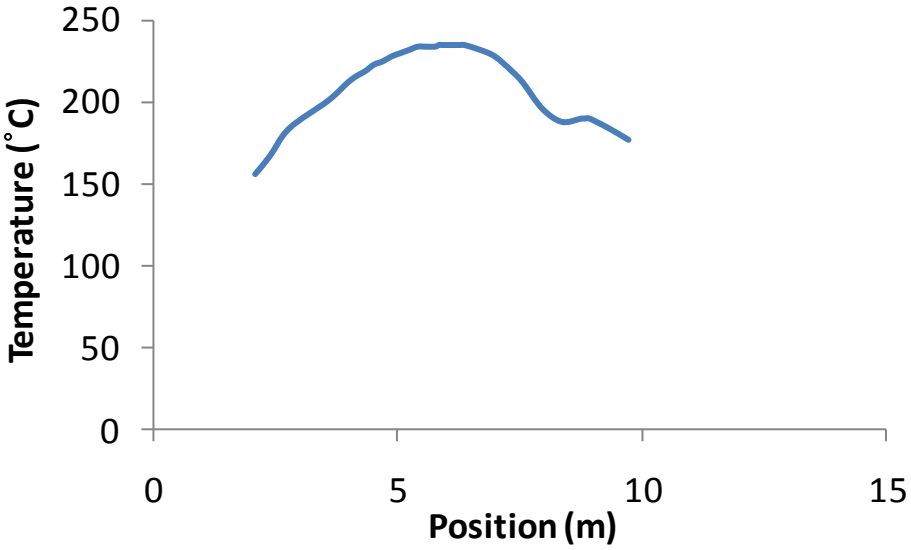

Figure 2-3. The temperature profile of the side of the core barrel.

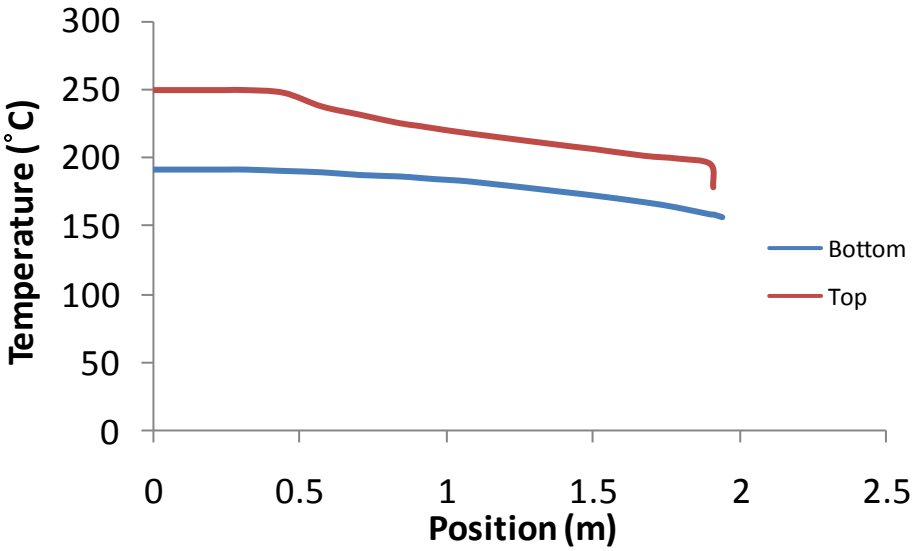


Figure 2-4. The temperature profile of the top and the bottom of the core barrel.

Table 2-1 HTR-10 design primary system parameters [1]

| Parameters | Unit | Value |
|---|---|---|
| Thermal power | MW | 10 |
| Primary helium pressure | MPa | 3.0 |
| Inlet helium temperature | ℃ | 250 |
| Outlet helium temperature | ℃ | 700 |
| Primary coolant flow rate | kg/s | 4.3 |
| Outlet steam pressure at the S.G | MPa | 4.0 |
| Outlet steam temperature at the S.G | ℃ | 440 |
| Secondary steam flow rate | kg/s | 3.47 |
| Core volume | $m^3$ | 5.0 |
| Core diameter | m | 1.80 |
| Core height (Average) | m | 1.97 |
| H/D ratio | | 1.09 |
| Diameter of fuel element | cm | 6 |
| Number of fuel elements | | 27,500 |
| Burn-up (Average) | MWD/T | 80,000 |

S.G refers to the steam generator

# CHAPTER 3
# COMPUTATIONAL FLUID DYNAMICS

## What Is Computational Fluid Dynamics (CFD)?

The behaviors of the fluid can be solved by the Navier-Stokes equations which are derived from four equations:

- Mass Conservation
- Momentum Conservation
- Energy Conservation
- Equation of State

The Navier-Stokes equations become more complicated when the situation is larger than one dimension. The highly dimensional Navier-Stokes equations cannot easily be analyzed by regular processes, so numerical methods are used to solve the heat transfer problems. Programming using numerical methods to solve the Navier-Stokes equations has led to development of a number of codes, referred to as CFD codes which are powerful at researching in both fields of science and engineering. In the wake of developments in semiconductors and technology, computers can process more data and solve problems much faster and more accurately; moreover, the larger random-access memory (RAM) can store more data for accelerating calculations and saving time. Therefore, CFD has become a common numerical tool for solving the Navier-Stokes equations. In order to calculate with a CFD code, a grid is given along with the boundary conditions and physical models which will be discussed later. Generally, the geometry is divided into a large number of meshes with small size, and the CFD code then solves the governing equations for the unknown variables [8]. By iterating, the code finally gets either converged or diverged due to several reasons (mesh size, mesh shape, boundary conditions, and etc.). Generally speaking, the solutions get converged when the difference of the unknown values from one iteration to the previous are within $10^{-6}$.

## Governing Equations

To describe the governing equations, four parameters are listed below:

- Temperature T
- Velocity $\vec{v}$
- Pressure P
- Density ρ

A two-dimensional coordinate system is considered in this study. It is the (x, r) coordinate system where x is the axial direction and r is the radial direction. The water coolant's temperature does not reach the boiling point, so all fluids in the HTGR are considerate as the single-phase flow.

Mass Conservation: Continuity Equation

The continuity equation is given by

$$\frac{\partial \rho}{\partial t} + \nabla \cdot (\rho \vec{v}) = 0 \qquad \text{(Eq. 3-1)}$$

Eq. 3-1 is the general form of the continuity equation and is valid for both compressible and incompressible flows.

Momentum Conservation: Newton's Second Law of Motion

Newton's Second Law of motion is described by

$$\frac{\partial \rho \vec{v}}{\partial t} + \nabla \cdot (\rho \vec{v}\vec{v}) = -\nabla P + \nabla \cdot \bar{\bar{\tau}} + \rho \vec{g} + \vec{F} \qquad \text{(Eq. 3-2)}$$

For Eq. 3-2 describes $\bar{\bar{\tau}}$ is the stress tensor, $\rho \vec{g}$ and $\vec{F}$ are the gravity and external body forces, respectively. In this thesis, there are no external body forces, $\vec{F} = 0$, but gravity is considered and this results in natural convection of gases.

The stress tensor is given by

$$\bar{\bar{\tau}} = \mu[(\nabla \vec{v} + \nabla \vec{v}^T) + \frac{2}{3} \nabla \cdot \vec{v} I] \qquad \text{(Eq. 3-3)}$$

Energy Conservation: First Law of Thermodynamics

Energy Conservation is given by

$$\frac{\partial}{\partial t}(\rho E) + \nabla \cdot \left(\vec{v}(\rho E + P)\right) = \nabla \cdot \left(k_{eff}\nabla T - \sum_j h_j \vec{J}_j + \left(\bar{\bar{\tau}}_{eff} \cdot \vec{v}\right)\right) \quad \text{(Eq. 3-4)}$$

Energy E and enthalpy h are defined as follows:

$$E = h - \frac{P}{\rho} + \frac{v^2}{2} \quad \text{(Eq. 3-5)}$$

$$h = \int_{T_{ref}}^{T} C_{p,j}\, dT \quad \text{(Eq. 3-6)}$$

In the Eq. 3-6, $T_{ref}$ usually is room temperature, 298.15K (25℃).

Equation of State

The equation of state describes the relationship of density, temperature and pressure. Density is written as the simple equation $\rho = \frac{P}{RT}$, if the fluid is considered as a perfect ideal gas; if the fluid is considered incompressible, the density is regarded as a constant (ρ = constant).

## CFD Solver

CFD codes have different solver types:

- Pressure-based implicit
- Density-based implicit
- Density-based explicit

Each formulation is used for a different purpose. In an implicit formulation, for a given variable, the unknown variable in each cell is computed using both existing and unknown values from the neighbor cells; on the contrary, in an explicit formulation, the unknown variable is only computed using existing values. Therefore, in the implicit scheme, each unknown appears in more than one equation and all equations are solved simultaneously, whereas in the explicit scheme, the unknown variable appears in one equation and the equations are solved one at a time to get all the unknowns.

The explicit formulation is available only for the density-based solver. Both the pressure-based solver and density-based solver are able to select either a segregated or a coupled solution method. The segregated approach solves a single variable at a time, but the coupled approach

solves all variables at the same time. Generally speaking, the pressure-based approach and density-based approach were developed for different purposes; however, both methods have been modified to solve and operate for a wide range of flow conditions.

## Turbulence Modeling

Turbulent behavior of flows becomes significant due to the high Reynolds number. Turbulent flows are characterized by fluctuating velocity fields. These fluctuations, including contain transport properties, can be of small scale and high frequency. Furthermore, they are time consuming in computing as the simulation proceeds in practical engineering calculations. The simulations in the thesis are considered to be fully-developed turbulent flows; however, the water flow in the cooling pipe is a fully-developed laminar flow. Unfortunately, the FLUENT CFD code can only employ all turbulent or all laminar models in the same simulation, so the water flow is considered as turbulent flow like the helium and air flows. Two turbulent schemes, the realizable k-ε Model and the standard k-ω Model, in CFD codes were implemented in this thesis.

### Realizable k-ε Model

The realizable k-ε model is commonly chosen for a viscous model problem due to the advantage of providing similar simulation results in less time compared to other time-consuming models. [8] Also, this model presents the immediate benefit that it accurately predicts the spreading rate of planar and round jets, and seems to provide superior performance for flows under rotation, boundary layers with strong adverse pressure gradient, separation, and recirculation. The Bussinesq approach and the eddy viscosity definition are two principles of the realizable k-ε model used to solve the transport equations of the turbulent kinetic energy, k, and the dissipation rate, ε, described as:

$$\frac{\partial(\rho k)}{\partial t}+\frac{\partial(\rho k u_j)}{\partial x_j}=\frac{\partial}{\partial x_j}\left[\left(\mu+\frac{\mu_t}{\sigma_k}\right)\frac{\partial k}{\partial x_j}\right]+G_k+G_b-\rho\varepsilon-Y_M \quad \text{(Eq. 3-7)}$$

$$\frac{\partial(\rho \varepsilon)}{\partial t}+\frac{\partial(\rho \varepsilon u_j)}{\partial x_j}=\frac{\partial}{\partial x_j}\left[\left(\mu+\frac{\mu_t}{\sigma_\varepsilon}\right)\frac{\partial \varepsilon}{\partial x_j}\right]+C_{1\varepsilon}\frac{\varepsilon}{k}C_{3\varepsilon}G_b-\rho C_2\frac{\varepsilon^2}{k+\sqrt{\nu\omega}} \quad \text{(Eq. 3-8)}$$

$$G_k=-\rho\overline{u_i'u_j'}\frac{\partial u_j}{\partial x_i} \quad \text{(Eq. 3-9)}$$

$$G_b=\beta g_i\frac{\mu_t}{Pr_t}\frac{\partial T}{\partial x_i} \quad \text{(Eq. 3-10)}$$

They are the generation of the turbulent kinetic energy due to the velocity gradients and buoyancy, respectively; $Y_M$ is the fluctuating dilation in compressible turbulence considered for high Mach number flow, and is given by $Y_M = 2\rho\varepsilon M_t^2$.

Standard k-ω Model

The standard k-ω model, an empirical model based on the transport equations for the turbulent kinetic energy, k, and the specific dissipation rate, ω, includes low-Reynolds number effects, compressibility, and shear flow spreading. The k and ω equations have improved the accuracy for predicting free shear flows, and also been added the productions terms for modifications. To calculate the values of the turbulence kinetic energy, k, and the specific dissipation rate, ω, the transport equations are given by

$$\frac{\partial(\rho k)}{\partial t}+\frac{\partial(\rho k u_i)}{\partial x_i}=\frac{\partial}{\partial x_j}\left[\Gamma_k\frac{\partial k}{\partial x_j}\right]+G_k-Y_k \quad \text{(Eq. 3-11)}$$

$$\frac{\partial(\rho \omega)}{\partial t}+\frac{\partial(\rho \omega u_i)}{\partial x_i}=\frac{\partial}{\partial x_j}\left[\Gamma_\omega\frac{\partial \omega}{\partial x_j}\right]+G_\omega-Y_\omega \quad \text{(Eq. 3-12)}$$

where $\Gamma_k=\mu+\frac{\mu_t}{\sigma_k}$, $\Gamma_\omega=\mu+\frac{\mu_t}{\sigma_\omega}$, and $\omega=\frac{\varepsilon}{\kappa}$

$G_k$, $G_\omega$, $\Gamma_k$, and $\Gamma_\omega$ are the generation of turbulence kinetic energy due to mean velocity gradients, the production of ω, and the effective diffusivity of k and ω, respectively. The other two parameters, $Y_k$ and $Y_\omega$, represent the dissipation of k and ω due to turbulence. $G_k$ is given by Eq. 3-9 and the generation of ω, $G_\omega$, is giving by

$$G_\omega = \alpha \frac{\omega}{k} G_k \quad \text{(Eq. 3-13)}$$

The dissipations are described by

$$Y_k = \rho \beta^* f_{\beta^*} k\omega \quad \text{(Eq. 3-14)}$$

$$Y_k = \rho \beta f_\beta \omega^2 \quad \text{(Eq. 3-15)}$$

## FLUENT 6.3

As mention before, CFD has been widely used in solving thermal-hydraulics and heat-transfer problems, and has been used in nuclear technology including by National Laboratories [8]. FLUENT is CFD software developed by Fluent Inc- Lebanon, NH, and is commonly used at the Innovative Nuclear Space Power and Propulsion Institute (INSPI) due to the advantages of modeling complex geometries and solving heat transfer and fluid mechanics problems. Also, single-precision and double-precision solvers are available to for two-dimensional or three-dimensional problems. Single-precision is sufficiently accurate for the results, but certain problems involving high thermal conductivity ratios, complex geometries, and disparate length scales benefit from using a double-precision version. Before simulating in FLUENT, the geometry and mesh grids are generated by the software GAMBIT [4] discussed later in this chapter.

GAMBIT is the software from Fluent, Inc for creating the grid file read by FLUENT to check that all materials and elements created are positive. The user can set the solver, energy, viscosity, and radiation models. Boundary conditions, operating conditions, and both fluid and solid properties, such as density, conductivity, emissivity, thermal expansion coefficient, specific heat capacity, and etc., need to be set in the system as well. Then, the pressure in the system, temperature for initial conditions, and mass flow rate or velocity of the flows should be initialized before being ready to iterate. As the results get converged, FLUENT is can plot all

contours and profiles of the parameters which are examined for the reliability and reasonability. The profiles and data can be saved as text files where the values are able to be used in other software.

### Grid and Meshes

The geometry is made of thousands or millions of grids depending on the mesh size. The fine and small size grids are able to avoid diverged problems; however, a large number of grids require more time compared to large size grids. Also, the CPU computational ability directly affects the speed of meshing. Three steps are utilized to generate grids with Gambit 2.3. First, to design the geometry, the nodes, edges, surface, and volumes are specified. Then, to create the structure grids, the mesh size and the shape are available to be set. Finally, the continuum types and boundaries need to be defined and to be written out for use in FLUENT 6.3.

### User Defined Function (UDF)

The UDFs, written in C language, are convenient for the users who use FLUENT to define their boundary conditions and the properties of the parameters. For example, it is useful to create a profile for temperature changes with positions, conductivity changes with temperature, heat flux changes with position on the wall, time dependence and so on. Before using UDF files, they need to be either interpreted or compiled in FLUENT. To be loaded in FLUENT, UDFs must have an include statement for the udf.h file, be defined using the DEFINE macro supplied by Fluent Inc., and use and return the values in SI unit.

### Solution Controls

By default, FLUENT stores discrete values at the cell centers, and then the face values are interpolated from the cell center values. The condition is using an upwind scheme. The word upwind means that the value is derived from the magnitudes in the cell upstream relative to the direction of the normal velocity. FLUENT allows the users to choose from several schemes [9]:

first-order upwind, second-order upwind, power law, and QUICK. QUICK scheme, a weighted average of second-order-upwind and central interpolations of the variable, is employed to estimate higher-order values of the variables in quadrilateral and hexahedral meshes [9]. The methods are able to be selected under the discretization panel in solution control before starting to run a case.

## Checking Convergence

In every case, FLUENT saves and plots the residuals with all parameters: continuity, velocity, energy and turbulence. The residual storage records the difference of each variable between calculating at iteration N-1 and iteration N divided by the physical time step. When the criteria are below $10^{-3}$, it is considered to be converged. However, a higher criterion, $10^{-6}$ is considered for two variables: energy and dose-intensity. The criterion can be set lower to get more accurate results, but this will require more time to reach convergence. Figure 3-1, for example, shows the residuals versus iterations from calculations performed in this study.

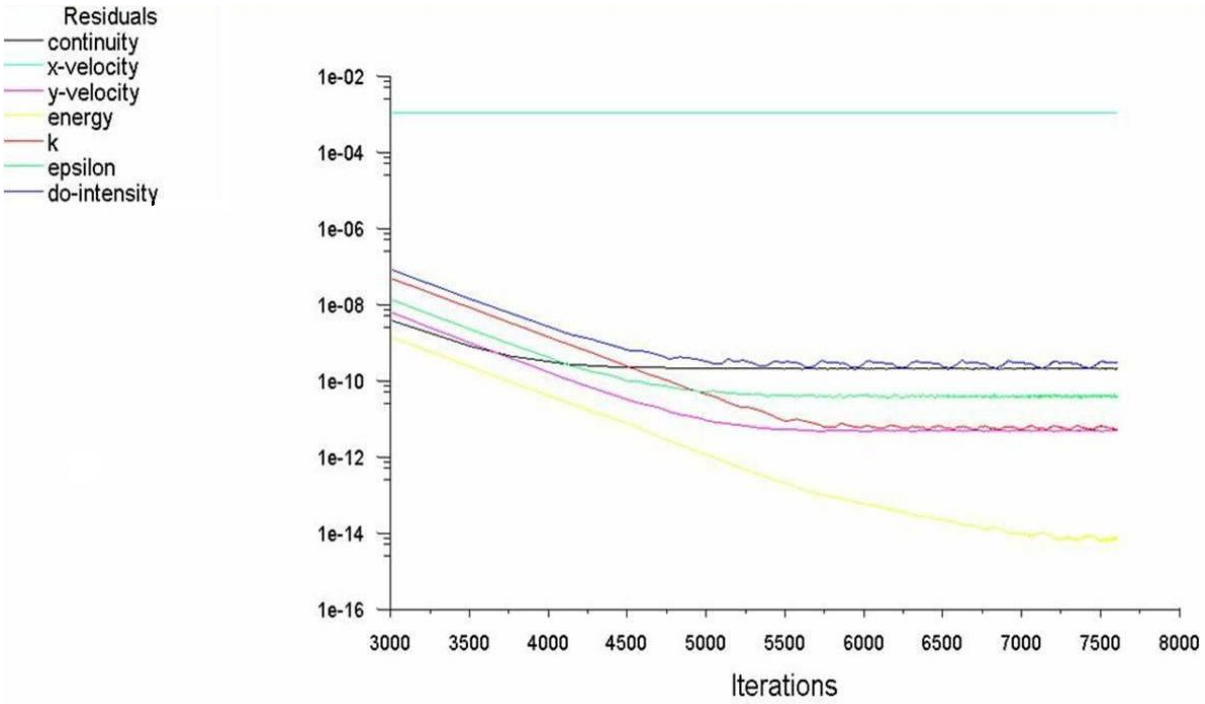

Figure 3-1. The residuals for seven variables versus iterations

# CHAPTER 4
# MODELING TECHNIQUE AND PHYSICAL PROPERTIES

## Data Sources

In order to reproduce the benchmark exercises, it was necessary to know the reactor and containment geometry, materials properties, operating conditions, and boundary conditions. These required data were provided in TECDOC 1163[1] in all categories except for containment geometry. So, the model geometry was mostly obtained from a schematic of the HTR-10 cross section presented by Gao and Shi [7]. In addition, some supplementary geometric data was obtained from the TECDOC 1163[1]. The TECDOC 1163 compiled CRP-3 [1] results summarize four benchmark exercises. CRP-3 [1] was done before the construction of the HTR-10 reactor, and the only data available are computer simulations.

The first challenge in reproducing the benchmark exercise is to correctly understand the geometry of the reactor, its components, the cavity and the RCCS. The description provided in the TECDOC [1] lack information. The missing dimensions are extracted from two sources, Gao and Shi [7] and Gao (1997) [6]. Both papers were published during or after the construction and these two main studies described the geometry information and materials characteristic of the HTR-10. The diagram in Gao's and Shi's report [7] presented the relative position of components inside the containment. Therefore, the height and radius dimensions were estimated to create the grids. Moreover, two flanges were added on the pressure vessel based on performance reported by Yu (2002). [10] The paper focuses on the flange performance, and also gives the details of the pressure vessel characteristic.

The second source of the material properties and operating conditions is the paper from Gao's, Lee's and Jiang's report in 1997 [6]. Moreover, the study from CRP-3 [1] includes the Gao's 1997 report [6] in its entirety, which also presented the details of the benchmark problem.

Gao reported the analytical results obtained with the 2-D transient thermo-hydraulic code THERMIX [6] that is powerful in calculating the material temperature. The main conclusion of the analysis was that the RCCS as initially designed removed too much heat from the core.

Gao published the report before the actual HTR-10 was built; therefore, some discrepancies between the data published and experimental data were presented in later publications. The data from Gao's 1997 [6] report are selected, and are compatible with the results of this thesis, which is the reproduction of the HTR-10 RCCS normal operation.

## The HTR-10 Geometry

Three physical structures of HTR-10 considered in this study are core barrel, the pressure vessel, and water cooling system. The dimensions of these components are shown as follows:

The pressure vessel

The HTR-10 the pressure vessel consists of a shell body, top closure, bottom closure and two flanges which connect the top closure to the shell body. Gao (1997) gives the dimensions of the pressure vessel shown in Table 4-1 [6].

However, Gao only mentions the total height of the pressure vessel without defining the height of the bottom closure. The total height of the pressure vessel given by Gao is 10.25 meters [6], which is different from the value of 11.16 meters height presented by Yu [10]. For this discrepancy, the schematic of the HTR-10 cross section is helpful to estimate the height of the bottom closure. Both Gao [6] and Wu [11] present the figure of the HTR-10 cross section, and the schematics show the length of the bottom closure is longer than the top closure. It means the length of the bottom closure is larger than 1.59 meters. If Gao's value is used, the height of the bottom closure will be 1.379 meters that is lower than 1.59. Therefore, the total height in Yu's

report was used [10], which is referred to 11.16 meters height, and the value of the bottom closure is 2.29 meters height.

Water cooling pipes (RCCS)

Two parallel water cooling systems are in the RCCS of HTR-10 surrounding the pressure vessel, located in front of the concrete wall of the containment. Each group, designed with a 125 kW heat removal rate, consists of 50 cooling tubes welded onto the annular plenum at the top and bottom of the reactor cavity. In the actual RCCS, these 100 discrete cooling pipes arranged in parallel have the dimensions given in Table 4-2 [6], run from the bottom to the top of the RCCS and discharge the decay heat to the chimney. An important drawback to represent the RCCS as a 2D-axisymmetric system is that the cooling pipes cannot be individually modeled. Hence, the discrete pipes had to be replaced by a continuous, axisymmetric water cooling wall that corresponds to a hollow cylinder of water, and the new diameter needed to be calculated for the 2D-axisymmetric model. Figure 4-1 illustrates that the idea of changing actual system to a 2D-axisymmetric system, but the 2D approximate method results in a less accurate simulation. To preserve some accuracy, the thickness of the axisymmetric cooling wall was calculated so that the mass flow area would be the same in the 2D-axisymmetric representation as in the actual HTR-10. The thickness of the new water wall is then equal to 4.2 mm, and the back of the cooling water wall was considered as a boundary because of ignoring the air and containment wall behind the cooling pipes.

Core barrel (Core vessel)

The dimensions of the core barrel, also named the core vessel, were obtained from TECDOC 1163 CRP-3[1] which only gives a half rectangular temperature profile without the exact position. The temperature profile is greatly useful in the 2D-axisymmetric model, and the

position of the core barrel in the pressure vessel was extracted from the graph in Gao's and Shi's report [6]. Moreover, CRP-3 [1] presents the top, side, and bottom lengths of the core barrel, and then the characteristic of the core barrel are estimated and listed in Table 4-3

## System Modeling

The HTR-10 RCCS benchmark exercises are code-to-code problems obtained from the CRP-3 [1]. A heatup experiment and a transient depressurized LOHS are the two scenarios, and both were simulated with FLUENT 6.3.26. Before simulating in FLUENT, the 2D axisymmetric model and grids were created by GAMBIT 2.3.16. The cross section of the model includes the core barrel, the pressure vessel, the surrounding containment, and water cooling pipes; three fluids were used in the simulations: the helium between the pressure vessel and the core vessel, air in the containment, and liquid water in the RCCS running from the bottom to the top. Figure 4-2A shows that the thickness and the external surface of the pressure vessel were present in the model, which is discussed in the "CFD Grids." Most of the heat was transferred from the pressure vessel to the RCCS through radiation, and a portion by natural convection. When heat is transferred to the RCCS, water removes heat to the chimney; then, heat dissipates into the atmosphere.

In the actual design, the RCCS are discrete pipes (Gao, 1997) [6], but the water wall was used in the FLUENT reproduction as shown in Figure 4-1. Behind the water wall is the concrete wall of the containment, and the concrete wall is not included in the modeling, which means the RCCS is the outer surface of the model. The dimensions used in the model are presented in Figure 4-2B.

## CFD Grids

Three models were created in the study used for heatup experiment and LOHS exercises, and were called Model 1, Model 2 and Model 3. Model 1 has the normal mesh element thickness

as 15 mm, which was separated in several parts for making perfectly rectangular or square grids in order to facilitate computation. A triangular grid can also be chosen in GAMBIT, but the triangular grids require more computation. As stated earlier, CRP-3 [1] gives the geometries to create Model 1 with a few more details added. To be more realistic, the water cooling wall was not completely straight, but had two 90° elbows at the inlet and outlet corners. The back of the water cooling wall was a boundary in these three models. Based on analyzing the HTTR-RCCS modeling, it was believed that the flange has important effects when the model included the flange. Therefore, Model 1 contained a flange on the pressure vessel wall; moreover, different thicknesses on the pressure vessel were taken into account as well. However, these realistic corrections increase difficulty for meshing grids and simulating in Model 1, so the third model is designed for the Depressurized LOHS accident.

In Model 2, two modifications have been made to the RCCS grid. First, the water cooling pipes in the model are now straight, spanning the entire length of the reactor cavity, because the elbows made it difficult to obtain a converged solution. Secondly, the mesh size was reduced from 15 mm to 5 mm to improve accuracy. Model 2 has better performance than Model 1, so the sensitivity study basically depended on this model.

Because LOHS is a transient exercise, the residuals have to be converged at the initial state first and then for changes with small time step. Model 3, designed for the transient case uses the same mesh size as Model 2 for accuracy, and was simplified in its structures. The pressure vessel was regarded as having no thickness for simplifying the model. In order to eliminate the thickness, the inner surface of the pressure vessel in the model was removed, but the flanges on the outer surface of the pressure vessel remained. This adjustment was due to the results of the sensitivity analysis. Depending on the sensitivity study, the complex structures made FLUENT

spend more time getting converged, and sometimes the results did not converge. One reason is believed that the mesh elements are not fine enough. The shape of the elements is not square but quadrilateral shapes. These poor elements make more computational difficulty and are led to diverged or keep steady. For example, Figure 3-1 shows the residuals did not get converged; therefore, to make sure the transient simulation works, Model 3 was optimized and simple.

## CFD Boundary Conditions and Physics Models

Boundary conditions were specified in FLUENT: the core barrel was set at the temperature profile specific to the benchmark exercise, the cooling pipe inlet was set at a specific mass flow rate and temperature, and all other boundaries were made adiabatic. There is an important distinction between the two benchmark exercises simulated: the heat-up experiment is at steady state, while the LOHS depressurization accident is undergoing a transient. Accordingly, the core barrel temperature profile and the inlet water temperature vary with time for the latter case. Boundary conditions were obtained from section 3.3.3 of the TECDOC [1].

Physics models in FLUENT were carefully chosen in order to make the benchmark exercises as accurate as possible; preliminary exercises were done before the benchmark exercises in order to choose the best physics models. The k- ω model was used to account for turbulent flow; the ideal gas law approximation was used to model density of the gases, and the discrete ordinates model was used to account for radiative heat transfer. The helium in the reactor the pressure vessel and the air in the reactor cavity are undergoing natural circulation, so normally the Boussinesq approximation would be used to model the density of these gases due to gravity. However, the radial temperature variations across these regions are on the order of 150℃, which are too high for the Boussinesq approximation to be valid. Besides these two approximations for modeling the density of gases, the incompressible ideal gas law was also used in the reproductions for the sensitivity analysis.

The k-ε turbulent model is widely known and used in the world, and it is easy to solve the govern equations and saves time. For the k-ω model, it was used for examining which turbulent model will provide the better performance in the sensitivity study, because to choose turbulent model is still a topic of much research. Furthermore, comparing the government equation of the k-ε model to the k-ω model, the latter simplified some terms, but basically the equations are very similar. Even though the equations of the k-ε model are close to the k-ω model, the solutions of these equations will not be the same due to the difference length scale. There is a k factor difference in both second dissipation equations, and all energy is finally dissipated by viscosity. The total amount of energy transfer must be equal to the dissipation rate, so the larger dissipation rate can remove more heat; therefore, to examine which turbulent model predicts a higher heat transfer rate is also an issue in this study as well. However, for the k-ω model, there is not much information, but at least the k-e model is known. It is invalid to use the k-ε model turbulent model in a very high Reynolds's number that also means the high eddy currents; another reason k-ε model was applied on this study is that the computation time is shorter, because the computational time is a major issue in CFD field.

**Materials Properties**

The core barrel, the pressure vessel, and the water cooling wall pipes are made of steel: SA387-11 and SA516-70 [1]. The relevant physical properties of these steels are the same; they are summarized in Table 4-4. The helium in the reactor pressure vessel and the air in the reactor cavity are set at an operating pressure of 1 atm. The temperature of helium and air are set to 523K and 350K, respectively. The remaining fluids properties were obtained from TECDOC [1] and can be found in Table 4-4. The emissivity of the core barrel, the pressure vessel, and the water cooling wall (i.e., all the steel components) were all set to 0.8; the emissivity for the adiabatic walls of the reactor cavity were set to 1.0. When the ideal gas law is used in FLUENT,

the density of gases is not required. Therefore, the helium and air density presented in Table 4-4 are only used for the Boussinesq approximation. In either the ideal-gas law or the Boussinesq approximation, the thermal expansion is required for calculating gases density, and the value is equal to one over temperature.

Table 4-1. Dimensions of the pressure vessel

| Component | Parameter | Value (m) |
|---|---|---|
| | Maximum outside diameter | 4.68 |
| | Inner diameter | 4.10 |
| Top closure | Closure thickness | 0.10 |
| | Total height | 1.95 |
| | Flange height | 0.60 |
| | Flange height | 0.60 |
| | Inner diameter | 4.10 |
| Shell body | Shell thickness | 0.07 |
| | Height of normal part | 2.882 |
| | Height of strengthen part | 3.80 |
| | Maximum outside diameter | 4.34 |
| Bottom closure | Inner diameter | 4.10 |
| | Closure thickness | 0.10 |

Table 4-2. Dimensions of the RCCS cooling pipes

| Parameter | Value (m) |
|---|---|
| Cooling tube length | 11.20 |
| Cooling tube outside diameter | 0.042 |
| Cooling tube inner diameter | 0.032 |
| Annular tube outside diameter | 0.152 |
| Annular tube inner diameter | 0.142 |
| Water cooling wall outside diameter | 6.090 |
| Water cooling wall inner diameter | 6.006 |

Table 4-3. Dimensions of the Core barrel

| Parameter | Value (m) |
|---|---|
| Half top length | 1.94 |
| Side length | 7.67 |
| Half bottom length | 1.94 |

Table 4-4. The material physical properties

| Material | Density | Specific Heat Capacity | Thermal Conductivity | Viscosity |
|---|---|---|---|---|
| SA387-11 | 8030 kg/m3 | 458 J/kg.K | 37 W/m.K | - |
| SA516-70 | | | | - |
| Helium-523K | 0.279 kg/m3 | 5193 J/kg.K | 0.152 W/m.K | 2.83e-5 kg/m.s |
| Air-350K | 0.995 kg/m3 | 1009 J/kg.K | 0.029 W/m.K | 2.082e-5 kg/m.s |
| Water | 998.2 kg/m3 | 4182 J/kg.K | 0.6 W/m.K | 1.003e-3 kg/m.s |

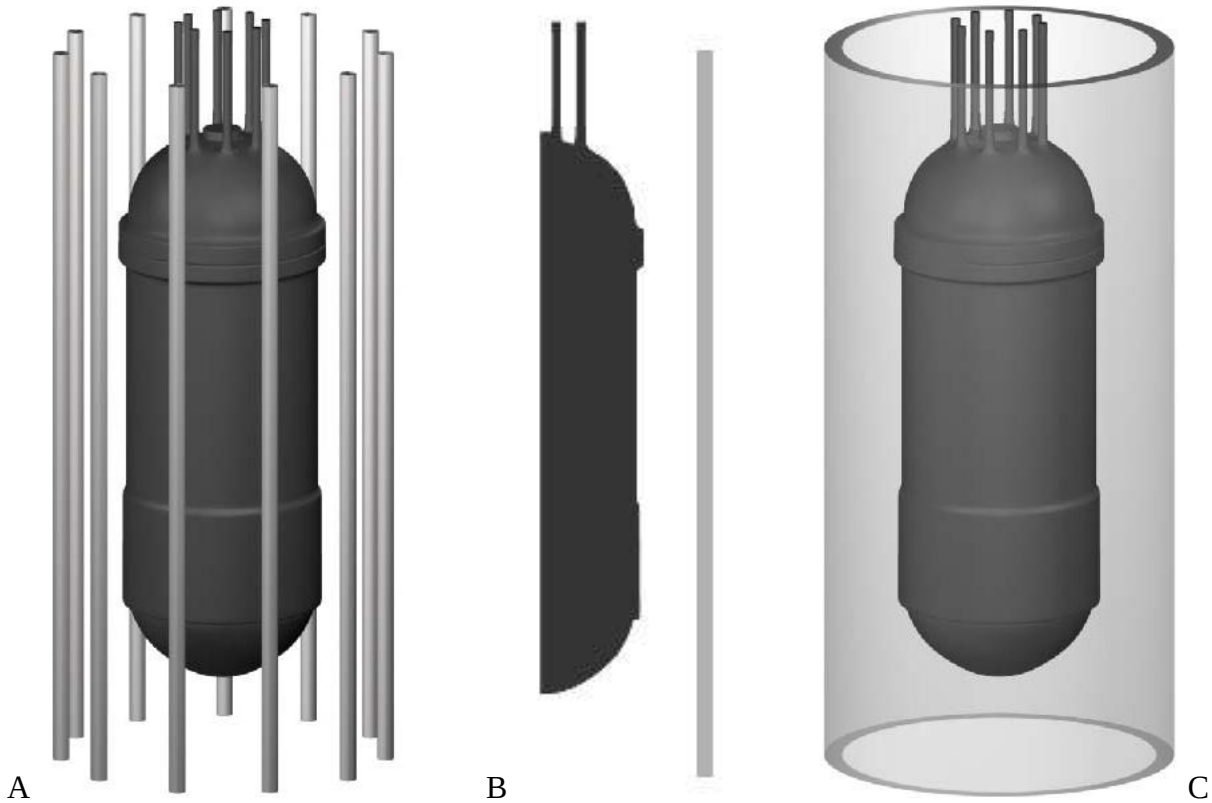


Figure 4-1. The RCCS representation. A) Actual system. B) 2-D axisymmetric model. C) 2-D axisymmetric system representation.

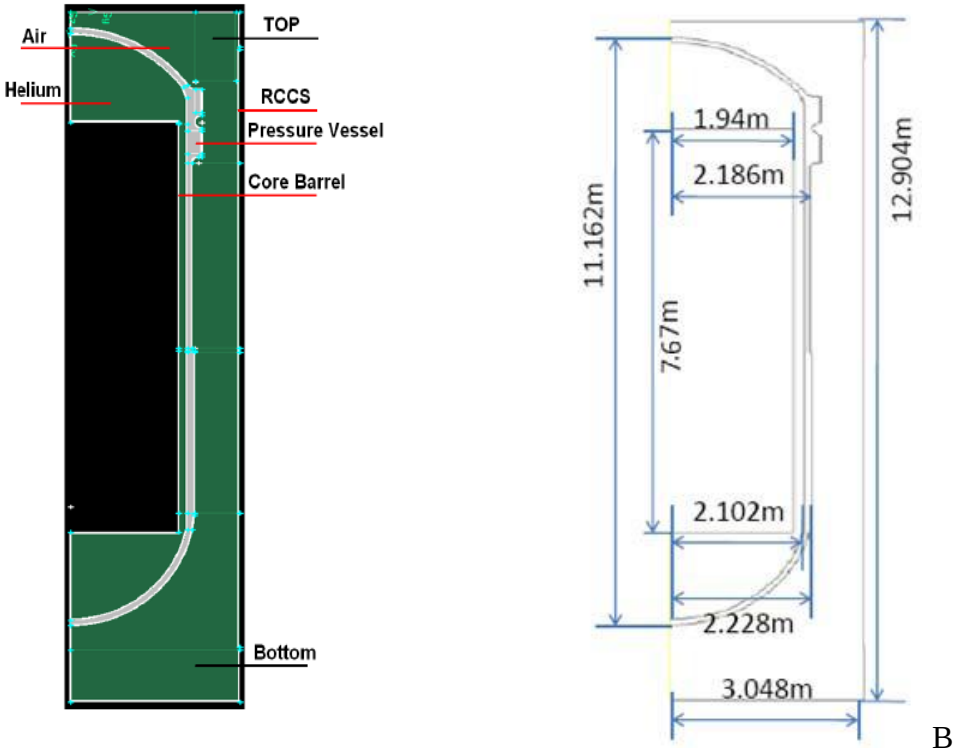


A B

Figure 4-2. The HTR-10 cross section in Model 1. A) Material position and structure modeling. B) The specific dimensions of HTR-10 modeling.

# CHAPTER 5
# HAND CALCULATION

## Introduction

This study is used to analyze the local heat removal rate by the RCCS and the benchmark problems of the HTR-10. In the CRP-3 document, it was indicated that for the heatup experiment THERMIX predicted the heat removal rate was 215kW [1]. Because of discrepancies between THERMIX and FLUENT and because of modeling limitations in FLUENT, estimates were performed for the total heat transfer rate by using hand calculations. Because the problem setup is complicated, some assumptions were made such as: simplifying the geometry of the model, using uniform helium and air temperatures, uniform surface temperature of the core barrel, the pressure vessel, and the RCCS, and considering helium and air transferred heat via natural convection in the concentric cylindrical system and also by thermal radiation. The mean values were used as these uniform values, and the core barrel was separated into three parts: top, side, and bottom; therefore, three different average temperature values for the core barrel were taken into account in the calculation.

## Heat Transfer Rate Calculation

### Geometry Assumptions

First, the core barrel, which is a cylinder with a radius of 1.94m and a height of 7.67m, was divided into three parts: the top, the side and the bottom. Each part had uniform mean temperature values assigned based on the temperature distribution given in Table A.1 of CRP-3 [1]; they were 273.465K, 326.272K, and 202.367K, respectively. Secondly, the pressure vessel was made of two hemispheres and one cylinder with a radius of 2.102m and a height of 8.131m. These three parts had a total surface area of 162.91 $m^2$ and the same, uniform temperature. The third issue included two alternate situations: 1) where the RCCS was regarded as the actual

configuration of 100 discrete pipes, and 2) where the RCCS was considered as a cylindrical water wall with the radius of 3.0388 m. Moreover, the thickness of the pressure vessel and the RCCS were ignored and they were considered as opaque, gray and diffuse surfaces.

**Properties Assumption**

Because the thermal properties of the fluids are dependent on their temperature, another assumption was using linear interpolation between two temperature intervals to estimate the thermal properties of helium and air. In spite of using this assumption, the water flow was chosen with constant thermal properties and independent of the temperature changes.

The reference temperature for helium and air was set by the average temperature between the core barrel and water inlet, so the pressure vessel temperature was around 195℃; moreover, the helium and air temperature were guessed using the same method to get the average value as well. The reference temperature of the helium and air were 227℃ and 127℃, respectively. Once the reference temperatures were chosen, it was easy to define the parameters which were involved in the calculation of the heat transfer by natural convection. It was necessary to calculate the Rayleigh number to determine the convection heat transfer rate and the natural convection Rayleigh number equation for concentric cylinders is given in Eq.5-1

$$\boldsymbol{Ra_c} = \frac{g\beta(T_i - T_o)L_c^3}{\nu\alpha} \qquad \text{(Eq. 5-1)}$$

where the length scale in $Ra_c$ is given by

$$\boldsymbol{L_c} = \frac{2[\ln(r_o - r_i)]}{(r_i^{-3/5} + r_o^{-3/5})^{5/3}}\,. \qquad \text{(Eq. 5-2)}$$

**Heat Transfer Calculation**

Heat is transferred from the core barrel to the RCCS, and then removed by water coolant flow. In the heat transfer calculation, the first step was to divide the problem into three sections: heat transfer from the core barrel to the pressure vessel, from the pressure vessel to the RCCS,

and from the RCCS to the water coolant. The known property values are given in Table 5-1. The next step was to solve for the total heat transfer rate which included radiation and natural convection but no conduction for two reasons: there is no thickness in the solids, and the conductivity of the fluids is too low. Subsequently, the natural convection heat transfer rate was obtained by using Eq.5-3 and Eq. 5-4 and also by using Eq. 5-1 and Eq. 5-2 for $Ra_c$ [12]:

$$\boldsymbol{q = \frac{2\pi L K_{eff}(T_i - T_o)}{\ln(r_o/r_i)}} \quad \text{(Eq. 5-3)}$$

where $K_{eff}$ is defined as the following

$$\boldsymbol{K_{eff} = K * 0.386\left(\frac{Pr}{0.861+Pr}\right)^{4/3} Ra_c^{1/4}} \ . \quad \text{(Eq. 5-4)}$$

The radiation heat transfer rate utilized the view factor, the surface temperature, and material emissivity; Eq. 5-5 shows the relation of the radiation heat transfer [13]. As mentioned above, the core barrel was separated into three parts, so the heat transfer rate was the summation of contribution from these parts.

$$\boldsymbol{q = \frac{\sigma(T_1^4 - T_2^4)}{\frac{1-\varepsilon_1}{\varepsilon_1 A_1} + \frac{1}{A_1 F_{12}} + \frac{1-\varepsilon_2}{\varepsilon_2 A_2}}} \quad \text{(Eq. 5-5)}$$

**Results and Discussion**

**Heatup experiment**

When the temperature profile given in Table A.1 from CRP-3 was used, the calculated heat transfer rate using the water wall was 235.36 kW, within 9.46% of the THERMIX value of 215 kW [1]. Furthermore, the heat transfer rate was smaller if the water cooling wall was replaced by discrete water pipes; the value was calculated as 196.58 kW, within 8.56% of the THERMIX prediction. (Table 5-2) Because THERMIX is a 1-D heat transfer simulation, a problem might be that the axial direction of the radiation was not considered. If the top and the bottom surfaces of the core barrel are not taken into account in the computation, the total heat transfer rate was calculated to be 223.05 kW using the water wall, within a difference of 3.74% of the THERMIX

value. When the discrete pipes condition was considered, a calculated value of 190.64 kW was obtained and the difference was within 11.33% of THERMIX.

However, the temperature distributions are different in Table A.1 and Figure 3.36 of the CRP-3, which will be discussed in Chapter 6 [1], so the Figure 3.36 temperature profile was used for a second set of calculations that also provided two answers for the water wall configuration: with or without the top and the bottom core barrel surfaces. The heat transfer rates with and without the surfaces were 274.85 kW and 265.99 kW, respectively, and these results will be compared with those predicted by FLUENT. For the discrete water pipe configuration, the calculated results were 229.55 kW and 227.33 kW, with and without the top and bottom core barrel surfaces, respectively.

After calculating, the temperature of the helium, the air, the pressure vessel and the RCCS were 252.0℃, 142.25℃, 213.7℃ and 70.79℃, respectively. For the calculated and reference temperature, the difference of the helium and air were 25℃ and 10℃ degrees and the corresponding difference in the thermal properties was within 7%. According to the results, the highest total heat transfer rate was 274.85 kW and the lowest was 190.64 kW. For a total heat removal rate of 274.85 kW the water temperature difference is 12.584℃. For a total heat removal rate of 190.64 kW, the water temperature difference is 8.73℃. By comparison, a THERMIX value of 215 kW is given in the CRP-3 document [1]. CRP-3 indicates the RCCS was designed to have the heat removal ability of 250 kW in the HTR-10 design, so the THERMIX prediction was not over the design limitation; however, the calculated values exceeded the limitation in some cases.

**LOHS depressurized accident**

The temperature distribution for the LOHS accident is also given in the CRP-3 document. From the hand calculations, 112.53 kW and 99.462 kW were the results estimated with the water cooling wall. For the discrete pipes condition, the calculated values were 94.041 kW and 85.031 kW (Table 5-2). Whether the top and the bottom surface of the core barrel was included in the computation or not, the difference between the two water cooling configuration results was within 16%. These hand calculated results showed that when the reactor is under the LOHS accident, the RCCS has the ability to remove around 100 kW of heat. The CRP-3 indicated the initial reactor thermal power was 224 kW in the LOHS accident, so the heat removal rate was about one-half in the benchmark problem. The calculated values will be discussed with the FLUENT prediction in the next chapter. All parameters can be found in Appendix A.

The two different water cooling configurations resulted in different heat transfer values. Whether the top and the bottom surfaces of the core barrel were considered in the computation or not, these two water cooling configurations gave a difference within 16.5%. This means that the water coolant wall can remove 16.5% more heat than the discrete water pipes in both the heatup experiment and the LOHS accident, and this is reasonable due to the total surface area. The water wall has a larger total surface for heat transfer to the RCCS, and the 100 discrete pipes have a smaller area; therefore, the water wall has higher removal heat ability. However, in the actual design, to create water cooling wall is more difficult than the discrete pipes, but the discrete pipes calculation will be more reliable.

## Decay Power Calculation

Theoretically, after shutdown the reactor still generates heat that is the decay heat is due to the delayed neutrons, the beta decay, and the gamma ray decay. The decay heat rate due to beta and gamma decay is given by [14]

$$\frac{P}{P_0} = \mathbf{0.066}[(\tau - \tau_s)^{-0.2} - \tau^{-0.2}] \quad \text{(Eq. 5-6)}$$

where $\tau - \tau_s$ and $\tau$ are the time intervals in seconds after the reactor shutdown and after reactor startup, respectively.

The decay heat due to delayed neutron fission is given by

$$\frac{P}{P_0} = \frac{\beta(1-\rho)}{\beta-\rho} e^{-t/T_{asy}} \quad \text{(Eq. 5-7)}$$

where $T_{asy}$ is the asymptotic period of 80.645 seconds, and t in Eq. 5-7 is in seconds.

The LOHS benchmark problem described that the reactor lost its primary helium coolant and the thermal power decreased to 224 kW and then shut down automatically [1]. The lowest RCCS heat removal rate was estimated to be 94 kW (Table 5-2). Figure 5-1 shows the total decay heat as a function of time using Eq. 5-6 and Eq. 5-7, and appendix B provides the data. Also, Hu and Wang [15] gave the reactivity value of negative 8.86% when the reactor was shut down. Assuming that the delayed neutron constant was 0.007, from Eq. 5-7, the prompt drop of the decay heat was calculated as 17.85 kW which is far lower than 94 kW heat removal rate. Moreover, assuming the reactor has been operated for one year, from Table B-1, the total decay power reaches the value of 94 kW within merely a few seconds, which means that the RCCS can remove all decay heat after reactor shutdown. Hence, one is able to say that the RCCS has the ability to maintain the reactor safely due to the RCCS high heat removal rate.

Table 5-1. Fluid properties and assumption [1]

| Material | Parameter | Value | Unit |
|---|---|---|---|
| Water coolant | Specific heat capacity | 4184 | J/K/kg |
| | Inlet temperature | 64.5 | ℃ |
| | Mass flow rate | 5.22 | kg/s |
| Core barrel | Top temperature | 273.465 | ℃ |
| | Side temperature | 326.272 | ℃ |
| | Bottom temperature | 202.367 | ℃ |
| Helium* | Temperature | 227 | ℃ |
| | Expansion coefficient | 0.0020 | 1/K |
| | Specific viscosity | 290*10^-6 | $m^2/s$ |
| | Thermal conductivity | 0.22 | W/m/k |
| | Thermal diffusivity | 434*10^-6 | $m^2/s$ |
| Air* | Temperature | 152 | ℃ |
| | Expansion coefficient | 0.00235 | 1/K |
| | Specific viscosity | 29.4*10^-6 | $m^2/s$ |
| | Thermal conductivity | 0.03555 | W/m/k |
| | Thermal diffusivity | 42.75*10^-6 | $m^2/s$ |

* means the fluid is using the reference temperature

Table 5-2. The results of the hand calculations in different cases.

| Benchmark problem | Water coolant | Top and bottom of the core barrel | |
|---|---|---|---|
| | Type | With | Without |
| Heatup temp. from table | Water wall | 235.36 kW | 223.05 kW |
| in CRP-3 | Discrete pipes | 196.58 kW | 190.64 kW |
| Heatup temp. from figure | Water wall | 274.85 kW | 265.99 kW |
| in CRP-3 | Discrete pipes | 229.55 kW | 227.33 kW |
| LOHS accident | Water wall | 112.53 kW | 99.462 kW |
| | Discrete pipes | 94.014 kW | 85.031 kW |

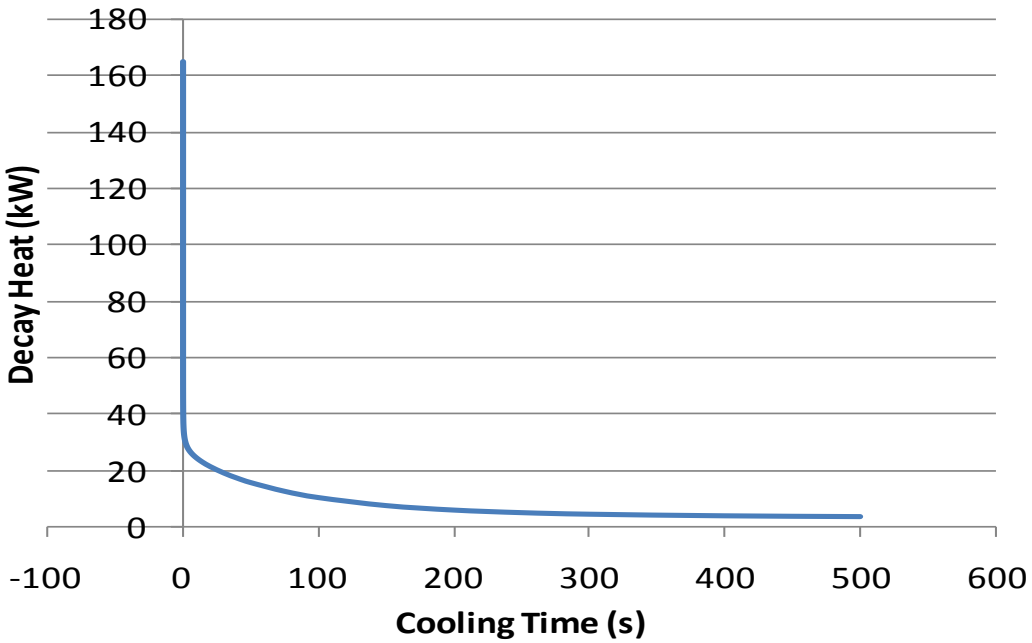

Figure 5-1. The total decay heat with the cooling time.

# CHAPTER 6
# SIMULATIONS AND RESULTS

The heatup experiment and Loss of Heat Sink scenarios are modeled with FLUENT. TECDOC 1163 [1] provides the axial and radial temperature profiles on the core barrel for the heat up experiment (Figure 2-2), a set of profiles at different times for the LOHS, and the evolution of the RCCS inlet temperature with time. The profiles of temperature on the core barrel were implemented in FLUENT as the boundary condition. The predictions of the FLUENT reproductions are compared with the CRP-3 [1] simulations. The comparison of the benchmark exercises between FLUENT and THERMIX is discussed in the following.

## Heatup Experiment

In this scenario as described in TECDOC 1163[1], the HTR-10 reactor operates at the power of 200 kW. The RCCS water mass flow rate is 5.22 kg/s with the inlet temperature of 64.5℃. Because the analysis gears towards the study of the heat removal by the RCCS, the details of the core are not represented in the CFD model. TECDOC 1163 p. 83[1] provides discrete temperature data on the surface of the core barrel as a function of position, so an input file written in C-Language is necessary for use as a UDF. Linear interpolation was used for calculating the temperature in each element between two positions on the surface of the core barrel. The top, bottom and side temperature distributions were implemented in the same manner, and were written in the same C-file, because FLUENT can only compile one file at one time. Figure 6-1 shows the C-file where only the top part temperature is presented.

### Reproduction of Temperature Profile Given in the Table in CRP-3

### Simulation 1 in Model 1 with 15mm mesh size

Model 1 was implemented in the reproduction, and four models were set: the implicit pressure based is the solver, the Boussinesq approximation accounts for the density of the flows,

the realizable k-ε model is the turbulence model, and the energy radiation model uses Discrete Ordinates. This FLUENT calculation converged after 10600 iterations with a total heat transfer rate from the core vessel of 273.524 kW with the water temperature difference of 11.0℃. According to the results of THERMIX from CRP-3 [1], the heat removed by the RCCS was 215 kW with the water temperature difference of 9.9℃ rather than 11.0℃. [1] Figure 6-2 shows the temperature profiles obtained by THERMIX as well as those obtained by FLUENT. Some discrepancies presented in Figure 6-2 need to be considered. First, the temperature input on the core barrel of FLUENT should agree with the profile of THERMIX because of the boundary condition; however, the temperature profile shown in Figure 6-2 does not match with the distribution in Figure 2-2. Secondly, the maximum temperature difference of the core barrel between the results of THERMIX and FLUENT was 80℃, and the same issue also happened on the pressure vessel. Hence, it is obviously assumed that THERMIX used a different temperature profile on the core berrel than the one from the benchmark problem definition (Figure 2-2). Subsequently, the temperature distibution at the end of the core barrel in THERMIX (Figure 6-2) was abnormally low at a temperature of 100℃. There is no doubt that the temperature in either the core barrel or the pressure vessel was much higher than 100℃. The new temperature distribution of the core barrel given in Figure 6-2 was therefore utilized in the next simulation instead of the profile in Figure 2-2.

**Simulation 2 in Model 1 with 15mm mesh size**

The second simulation used the same models: pressure based solver, mesh size, turbulent, radiation, and density model. The THERMIX temperature profile of the core barrel extracted from Figure 6-2 was utilized as the new boundary condition. The new side temperature of the core barrel was implemented in the simulation because Figure 6-2 displays only the side temperature profile of the core barrel without the top and the bottom. For the temperature profile

on the top and the bottom, a new assumption was taken into account. The same temperature data, given on p.83 in TECDOC 1163[1], were used for the temperature distribution on the top and bottom. With this assumption the new temperature profile of the core barrel was defined and was used in Simulation 2. FLUENT provided the results in Figure 6-3 which shows higher compatibility than in Figure 2-2 where comparing with THERMIX. FLUENT predicted lower temperature profiles for the pressure vessel for most of the pressure vessel length, and the difference was within 30℃; it reached nearly 40℃ at the flange located at 2 m. Regarding this large temperature difference at the flange location, it is possible that the THERMIX simulation did not include the pressure vessel flanges. The flanges are at a lower temperature than the rest of the pressure vessel because they increase the thickness of the pressure vessel. Also, the flanges have a larger surface area available for heat transfer to the RCCS. The temperature of the cooling wall was within 10℃ for nearly the entire pipe length, with some inconsistencies at the inlet and outlet. Furthermore, FLUENT showed a higher heat transfer rate but a lower maximum temperature on the pressure vessel than THERMIX. The heat transfer rate and the water temperature difference were 360.415kW and 15.5℃, respectively. It is reasonable that the second simulation predicted a higher heat transfer rate than Simulation 1, because the higher temperature profile of the core barrel was used as the boundary condition. The data for the maximum temperature and the cooling water outlet temperature are available in Table 6-1. Figure 6-4 provides the velocity profile from the model, and the side of the outer pressure vessel and the RCCS where velocity was extremely high should be noticed. FLUENT predicted the high velocity due to the complicated structures or mesh grids, so fine meshes were implemented in Model 2. The finer mesh size was made for improving the accuracy.

**Reproduction of Temperature Profile Obtained From the Figure in CRP-3**

**Sensitivity analysis- results**

Model 2 was used in the reproduction and the sensitivity analysis of the HTR-10 heatup exercises. Table 6-2 lists all simulations for the sensitivity study with two kinds of variables changed, but only four trials converged. Only discrete ordinates for the radiation model converged, so the radiation sensitivity analysis is not discussed. The other four reproductions listed in Table 6-3 are where the radiation model, mesh size and the solver were not changed but the turbulent and the density models were changed. After the study in Model 1, the core barrel temperature distribution in Figure 6-2 was used as the boundary condition instead of the distribution from Figure 2-2. Also, linear interpolation was used for calculating the temperature profile.

FLUENT was used to obtain results for four trials described as follows: Trial 1 gave a heat transfer rate of 360.062 kW with a water temperature difference of 14.5℃. The first trial used the realizable k- ε turbulent model and the Boussinesq approximation for density. Trial 2 was the reproduction with the realizable k- ε turbulent model and ideal-gas law for density. It gave a heat transfer rate of 328.916 kW and the difference of water temperature was 14.5℃. Trial 2 spent 49400 iterations and 223 hours to converge. The third trial gave a heat transfer rate of 348.013 kW with the water temperature difference of 15.4℃ using the k- ω turbulent model and ideal-gas law for density. Trial 3 took 33390 iterations and 102 hours to converge. The computational time compared to the other trials was half the value due to the use of a parallel processor. The parallel processor uses two or more CPU cores at the same time and is available to save computational time. Subsequently, Trial 4 spent 152 hours and 39100 iterations to converge and gave a heat transfer rate of 346.780 kW and a water temperature difference of 15.8℃. The incompressible ideal-gas law was used to model density and the k- ω model was used to account for turbulence

in Trial 4. Table 6-3 and Table 6-4 give more information and data of the trials. Moreover, if Trial 3 is chosen as the reference result, the differences were within 5.5% of what is predicted by Trial 2 and within 0.35% of Trial 4.

**Sensitivity analysis- discussion**

Even though Trial 1 gave the same order temperature distribution as the other trials, the Boussinesq approximation is not recommended to model the density of flows. As mentioned before, the Boussinesq approximation is valid for small differences of temperature. Consequently, it could lead to high errors because the temperature variations are on the order of 150℃ as demonstrated in Trial 1. An inconsistency shown in Table 6-4 is that Trial 1 predicted the highest heat transfer rate of 360 kW, but the lowest temperature value on the pressure vessel, cooling wall and water outlet; this behavior was dissimilar compared to the other trials. It is assumed that the Boussinesq approximation for density modeling led helium and air to contain more heat; in other words, helium and air in Trial 1 removed more heat than in the other trials. Based on Trial 1 and Trial 2, the only difference was the density modeling, and they predicted roughly the same temperature; however, the latter predicted a lower heat transfer rate by 30 kW. Despite of the 30 kW lower heat transfer, the temperature had the same behavior. Hence, it is believed that the ideal-gas law correctly models the lower heat removal ability. Because the ideal-gas law is more accurate in high temperature and low pressure conditions, the ideal-gas law is implemented in the modeling due to the high temperature in the reactor. The ideal-gas law for modeling the density is more correct than the Boussinesq approximation.

Besides Trial 1, the rest of the trials were discussed because the Boussinesq approximation was not proper for the simulations. According to the results of the experiments, Trial 3 gave the highest heat transfer rate, and Trial 4 predicted the highest temperature distribution on the pressure vessel and the RCCS. Table 6-4 shows the heat transfer rate increased by 19.1 kW when

the turbulent model was changed from the realizable k- ε model to the standard k-ω model. The difference was a 1.23 kW decrease when the incompressible ideal-gas law was substituted for the ideal-gas law. Trial 2 and Trial 3 were defined as the study in the turbulence sensitivity; Trial 3 and Trial 4 were regarded as the study in the density sensitivity. Depending on the sensitivity analysis, the difference of the heat transfer rate was larger in the turbulence change than in the density change. It is postulated that the incompressible ideal-gas law could perform about equally to the ideal-gas law for the heat transfer rate, but the turbulence model is the problem. Even though the density model of incompressible ideal-gas law predicted the same result, it is no doubt that the gases will be compressed. The effects in the incompressible ideal-gas law should be taken into consideration, and using the ideal-gas law for modeling density is more reasonable than the incompressible ideal-gas law. From the turbulence sensitivity analysis, the standard k-ω model provided better temperature distributions than the realizable k- ε model.

The sensitivity effects in temperature are analyzed as the following. These four reproductions gave similar results in the maximum temperature of the pressure vessel, of the cooling wall and of the water outlet. In Table 6-4, temperature of the pressure vessel increases from the Boussinesq approximation to ideal-gas law to incompressible ideal-gas law, and also increases from the realizable k- ε model to the standard k-ω model. Trial 1 and Trial 2 used the same turbulent model but changed the density model as did Trial 3 and Trial 4; temperature did not change obviously in the first two trials, nor for the last two trials. However, temperature changed dramatically in the turbulence sensitivity. Another influential fact is that the difference of the heat transfer rate was changed by 19.1kW when the turbulent model was changed, but the difference was merely 1.23 kW when another density model was used. It is believed that the modeling of flow density little affects temperature in the reactor, but the effects due to the

turbulent modeling were much greater. The same condition also happened at the water cooling pipes and water outlet, but they were not as significant. Table 6-4 shows temperature increased within 0.5℃ in the density sensitivity, and increased about 1℃ in changing the viscosity modeling. Based on the results of the trials, the maximum temperature on the pressure vessel agrees with the temperature of THERMIX within about 20℃. The maximum temperature in the RCCS was consistent with the value in TERMIX; Trial 4 in particular had only the difference of 0.6℃.

In general, FLUENT provided roughly the same values for the heat transfer rate in all trials with about 350 kW heat removed rate by the RCCS. However, the heat removal rate exceeded the value of 200 kW given in the heatup experiment. FLUENT predicted a higher heat transfer rate probably as a result of the temperature boundary condition. Hence, subsequent exercises were simulated which printed out the heat flux distribution of the core barrel and then normalized to 200 kW. When using a heat flux distribution as the boundary condition, the density-based solver is chosen due to the governing equations. Although the new concept was helpful, the results of each simulation diverged and no data are presented. Conclusively, the Boussinesq approximation and the incompressible ideal-gas law were not proper in the reproductions, so the use of ideal-gas law to account for density is a better model. In addition, the standard k-ω model gave better performance than the realizable k- ε model; therefore, Trial 3 was selected to be the reference model for the sensitivity analysis and was implemented for comparison with THERMIX.

**Comparing the Data between Trial 3 and THERMIX**

Trial 3 gave the better performance than others because of the advantages described above. Both temperature of the pressure vessel and the water pipes approached the results of THERMIX. Although Trial 4 gave less difference in temperature than Trial 3, the incompressible ideal-gas

law was believed to perform less accurately. In the turbulence modeling, the temperature distribution in the standard k- ω model was closer to the THERMIX results than in the realizable k- ε model. Based on these reasons, Trial 3 was used for comparing with the results of THERMIX.

The difference of the maximum temperature on the surface of the cooling pipes was within 1℃ between THERMIX and Trial 3. Figure 6-5 shows the comparison between THERMIX profiles [1] and FLUENT results of Trial 3. The pressure vessel temperatures were about 15℃ lower in the FLUENT predictions, with a maximum difference of 22.1℃ located where the profile peaks. The RCCS pipe temperature was within 0.6℃ for both simulations; more details are listed in Table 6-4. Depending on the design of the FLUENT model, the plus x-direction in Figure 6-5 is the direction from top to bottom in the actual geometry. In other words, the cooling water flowed in the negative x-direction in the model.

The same temperature profile for the core barrel was implemented in both THERMIX and FLUENT, but FLUENT predicted a heat removed rate of around 350 kW. The heat transfer rate given by FLUENT was larger than reported for the benchmark problem throughout the sensitivity analysis. The sensitivity studies did not reduce the heat transfer rate, but they gave approximately the same values for the temperatures. With the same temperature profile for the boundary condition, FLUENT never gets a heat transfer rate of 200 kW, and it is unreasonable that THERMIX showed a heat transfer rate of 200 kW. Based on the data obtained from CRP-3 [1], the temperature distribution is higher in the graph on p.93 than in the table on p.83. [1] The temperature profiles did not match each other, and it is believed that 200 kW came from the temperature profile of the table, and the data extracted from the figure would give more than 200

kW. However, FLUENT showed 273.524 kW in the previous simulation using the temperature profile from the table.

### Loss of Heat Sink (LOHS) Accident

The LOHS accident was a transient depressurized exercise operating at normal power condition of 10MW, and the water mass flow rate was 5.22 kg/s with the initial water inlet temperature of 50.4℃ [1]. The initial temperature of all the components is shown in Figure 6-6. The temperature profile of the core barrel is a function of position and time; also, the water inlet temperature is a function of time. In order to generate the temperature profile varying with time and position, a C-file is needed as the previous condition. The C-file used a 2D matrix to estimate temperature distribution results from three variables: position, time, and temperature. Figure 6-7 shows the partial contents of the temperature calculation in the C-file. FLUENT compiled this C-file to estimate the new temperature distribution corresponding to the current time for the transient simulations. The current time was changed by adding a small time step, once the residuals become converged. Then, FLUENT continued the new iterations until the residuals converge again due to the temperature perturbation and so on.

The transient reproduction utilized the optimized model from the sensitivity analysis. Model 3 was implemented in the LOHS exercise with the standard k-ω model, ideal-gas law, discrete ordinates, and pressure-based solver. The temperature data of the core barrel given on p.84-85 in CRP-3 [1] were used as the boundary condition. Roughly speaking, the temperature of the core barrel increases from an initial average temperature of about 210℃ to an average temperature of about 230℃ after 12 hours, and then it cools down over the next 108 hours. This is a rough description because of the different transient behavior at different parts of the core barrel, e.g. the bottom of the core barrel cools continuously from the initial to the final time. The inlet cooling water temperature starts at 50.4℃, and increases to about 51.0℃ over the first 12

hours; then decreases to about 46℃ over the next 108 hours. The time-dependent temperature profile at the cooling water inlet is displayed in Figure 6-8. On p.97 of CRP-3 [1] the temperature difference between the inlet and outlet of the cooling wall remained constant at 6.0℃ over the first 60 hours, indicating a constant heat removal rate; this temperature difference decreased over the second 60 hours of the transient [1]. However, FLUENT obtained a difference of 6.4℃ between inlet and outlet water temperature shown in Figure 6-8. Although FLUENT yielded a larger temperature change of 0.3℃ relative to THERMIX, a lower heat transfer rate was estimated in FLUENT. The cooling water outlet temperature predicted by FLUENT was within 0.5℃ of that predicted by THERMIX at the start of the transient given in Figure 6-9. Figure 6-9 also shows the temperature difference decreased with time.

Initially, FLUENT predicted a higher cooling water temperature, but a lower pressure vessel temperature. Between FLUENT and THERMIX, the temperature difference of any reactor or RCCS component was no more than 10℃. After 24 hours, this temperature difference increased to 17℃. Table 6-5 and Table 6-6 show the maximum temperatures of the reactor and the RCCS components at two times. The temperatures on the pressure vessel are lower in FLUENT than in THERMIX at both the initial state and at the 24th hour state. In addition, Table 6-5 and Table 6-6 show the temperature of the water pipes is larger at the beginning, but lower at the 24th hour state. The temperature profiles obtained by FLUENT at the initial time and the 24th hour are shown in Figure 6-10. The water pipe temperature decreased by14℃. Figure 6-10 shows that the maximum pressure vessel temperature has increased after 24 hours, as expected.

### 3-D Single Pipe Model

The FLUENT 3-D single pipe simulation examined a small slice of the whole reactor construction with only one single water cooling pipe which was one of the 100 total pipes; in other words, the 3-D reproduction had a 3.6 degree horizontal structure. The models used were

Discrete Ordinates for radiation, the pressure-based solver, the k-ω viscosity approximation for turbulence, and the incompressible ideal gas law for helium and air density; also, this calculation used the temperature profile obtained from Figure 3.36 of CRP-3 [1]. FLUENT predicted a total heat transfer rate of 2.181 kW with the water outlet temperature of 64.6℃, and the results are listed in Table 6-4. Thus, if the whole geometry were considered, the total heat transfer rate will be 218.1 kW which was close to the value of 229.55 kW from the hand calculation, within 5% difference.

The 2-D axisymmetric simulation was unable to represent the discrete water pipes and used the water cooling wall instead. Hence, the results of the 2-D axisymmetric calculation were compared with the results for same condition in the hand calculations. Trial 3 and Trial 5 showed the total heat transfer rate were 348 kW and 305 kW, respectively (Table 6-4); however, the value was 274.85 kW from the hand calculation. This means that the error was within 20% in Trial 3 which was the k-ω viscous model and the ideal-gas law, and was within 10% in Trial 5 that used the laminar approximation.

Comparing the 3-D model to the hand calculation, the difference of these two results is 11.45 kW with the error within 5% that shows the heat transfer rate predicted by FLUENT is in agreement with the analytical solutions. Although the 3-D model is powerful enough to predict better performance, it has some disadvantages, such as too much CPU time and memory requirements; therefore, a 2-D axisymmetric is used to simulate the real problem, but the 2-D model still has its own problem in that it removes more heat than the realistic situation due to the larger surface area.

To use a 3-D model is a better method to solve the problem, otherwise a 2-D axisymmetric is powerful as well. If a 2-D axisymmetric model is chosen, it is suggested to use the laminar

flow approximation and the ideal-gas law for density because of the lowest heat transfer rate prediction. This is to prevent overestimating the RCCS heat removal rate ability.

Overall, FLUENT predicts lower temperatures on the pressure vessel but higher water temperatures in both scenarios; this shows that FLUENT predicts higher heat exchanges between the RCCS and the pressure vessel than THERMIX. If more heat is transferred to the RCCS, the temperature on the pressure vessel will be lower. It is possible that FLUENT uses the larger radiation ratio than THERMIX, and emissivity probably affects the results. They are all set to 0.8 in FLUENT, but there is no information of the emissivity on the core barrel presented in the TECDOC [1]. Hence, two more sensitivity studies were run for estimation of emissivity effect. The first trial was the operating air temperature factor which was changed from 350° C to 400° C and the result indicated only a 2 kW difference. The second trial was the Trial 3 in the sensitivity analysis with the emissivity of the core barrel changed to 0.6 but the steel materials remained 0.8. The result showed a significant difference in which the heat transfer rate decreased by 27.8 kW.

```
#include "udf.h"
DEFINE_PROFILE(BarrelTopTemp,t,i)
{
 real y, x[ND_ND];     /* variable declarations */
 face_t f;

 int j, done;
 real vtemp;

 real T[20]={571,570.9,570.6,570.3,569.8,569.1,567.1,564.6,561.4,557.5,555.3,553.2,548,530.9,526.1,514.4,506.1,497.4,496.6,494.2};
 real height[20]={0,0.065,0.13,0.19,0.25,0.315,0.445,0.575,0.705,0.835,0.9,0.96,1.09,1.42,1.5,1.675,1.788,1.9,1.91,1.94};

 begin_f_loop(f,t)
  {
   F_CENTROID(x,f,t);
   y = x[1];
   done=0;
   j=0;

   while (done < 1)
   {
    if (y >= height[j] && y <= height[j+1])
      {
       vtemp= T[j] + (y-height[j])*(T[j+1]-T[j])/(height[j+1]-height[j]);
       done = 2;
      }
    else
     {j=j+1;}
    }

   F_PROFILE(f,t,i) = vtemp;
  }
 end_f_loop(f,t)
}
```

Figure 6-1. Example of UDF input file for the top temperature profile in the heat-up exercise

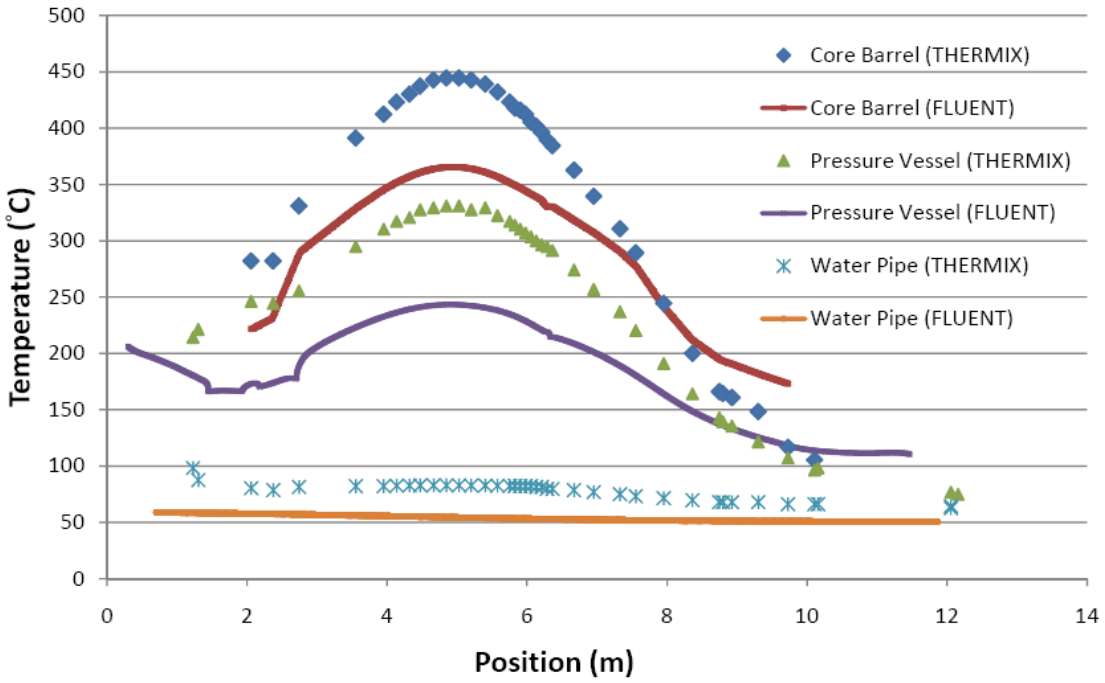


Figure 6-2. Temperature distributions of FLUENT and THERMIX for the heatup experiment in Model 1 with the boundary condition given from Table A1 of CRP-3. [1]

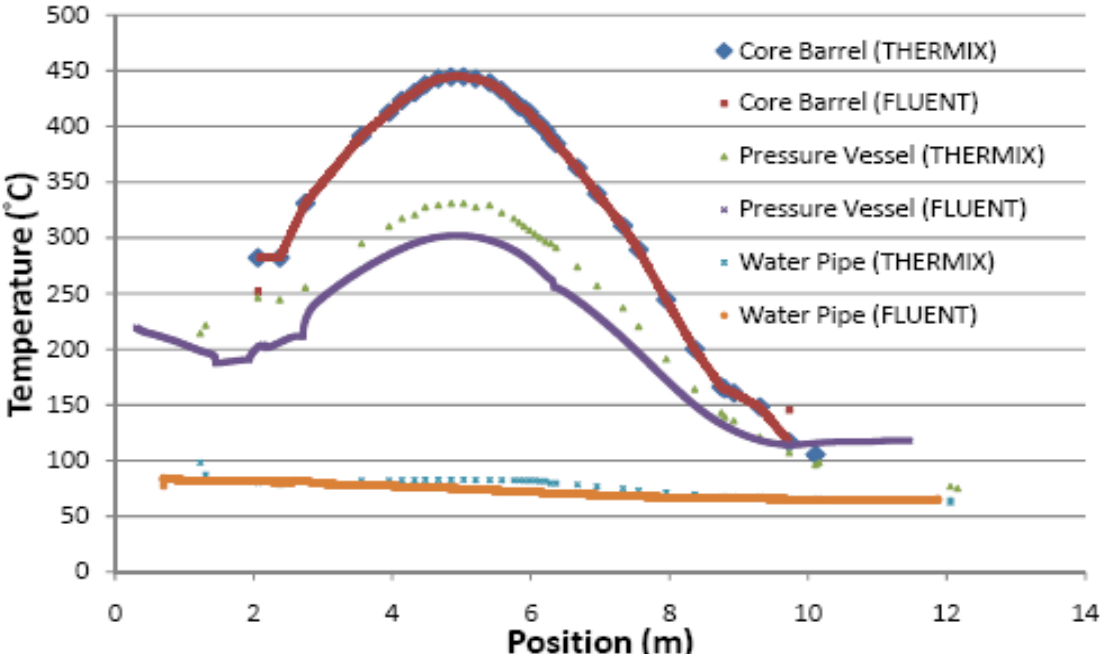


Figure 6-3. The velocity profile of simulation 2 in Model 1.

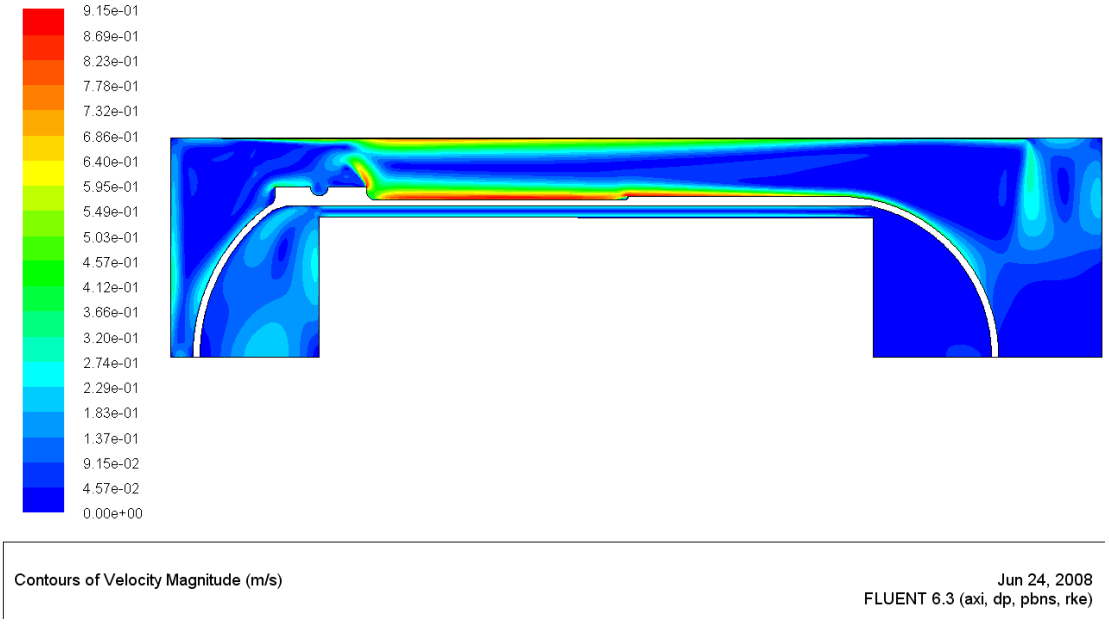


Figure 6-4. Temperature distributions of FLUENT and THERMIX for the heatup experiment in Model 1 with the boundary condition given from figure of CRP-3. [1]

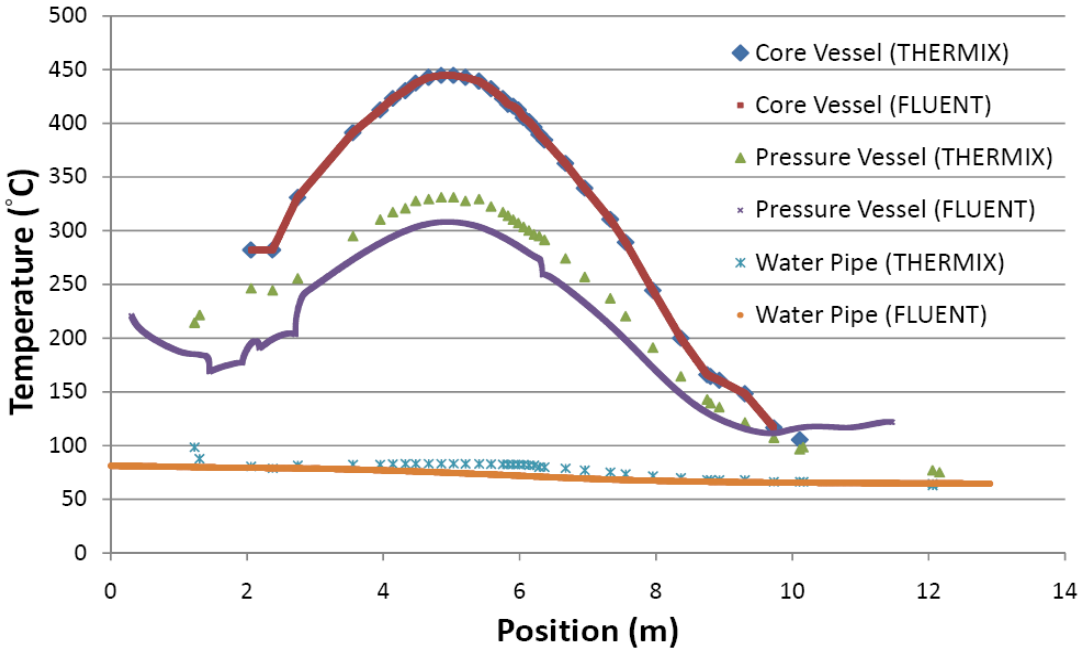


Figure 6-5. Temperature profiles of Trial 3 and THERMIX for the heatup exercise in Model 2

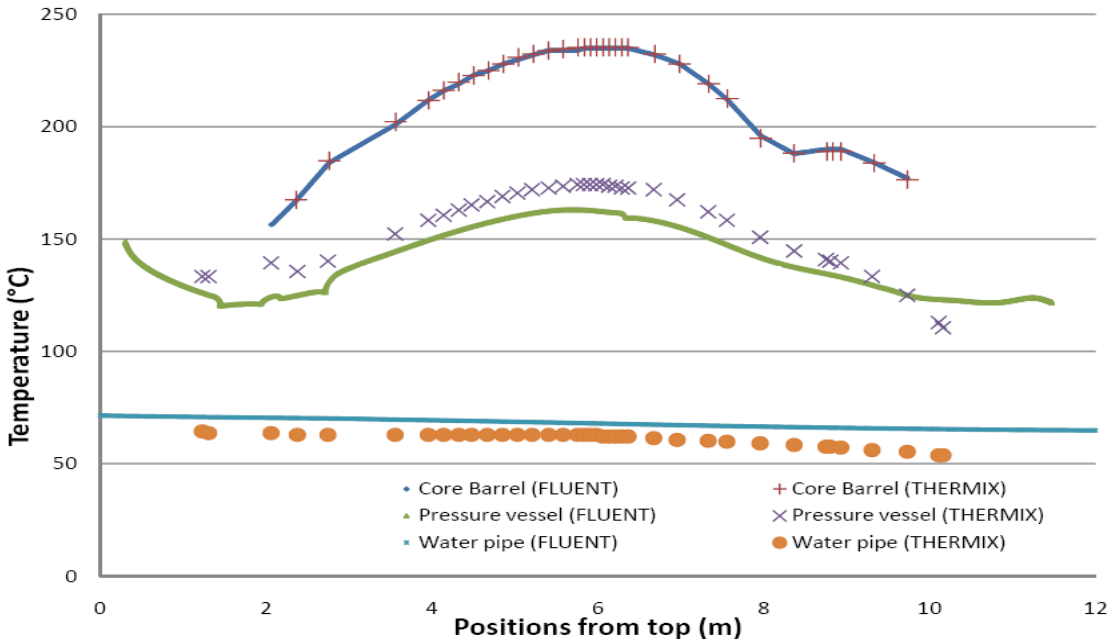


Figure 6-6. Temperature profiles of the LOHS accident for FLUENT and THERMIX at the initial state

```
begin_f_loop(f,t)
 {
  F_CENTROID(x,f,t);
  y = x[1];
  k= CURRENT_TIME;

  done=0;
  j=0;

  while (done < 1)
   {
    if (y >= height[j] && y <= height[j+1])
      {
            done2=0;
            j2=0;

      while (done2 < 1)
     {
       if (k >= time[j2] && k <= time[j2+1])
      {
       t1 = T[j2][j] + (k - time[j2])/ (time[j2+1]- time[j2]) * (T[j2+1][j] - T[j2][j]);
       t2 = T[j2][j+1] + (k - time[j2])/ (time[j2+1]- time[j2]) * (T[j2+1][j+1] - T[j2][j+1]);
       vtemp= t1 + (y - height[j]) * (t2 - t1) / (height[j+1] - height[j]);
       done2 = 2;
      }
      else
     {j2=j2+1;}
        }
         done = 2;
      }
    else
     {j=j+1;}
   }

  F_PROFILE(f,t,i) = vtemp;
 }
end_f_loop(f,t)
```

Figure 6-7. Example of UDF input file for the top temperature profile in the transient simulation

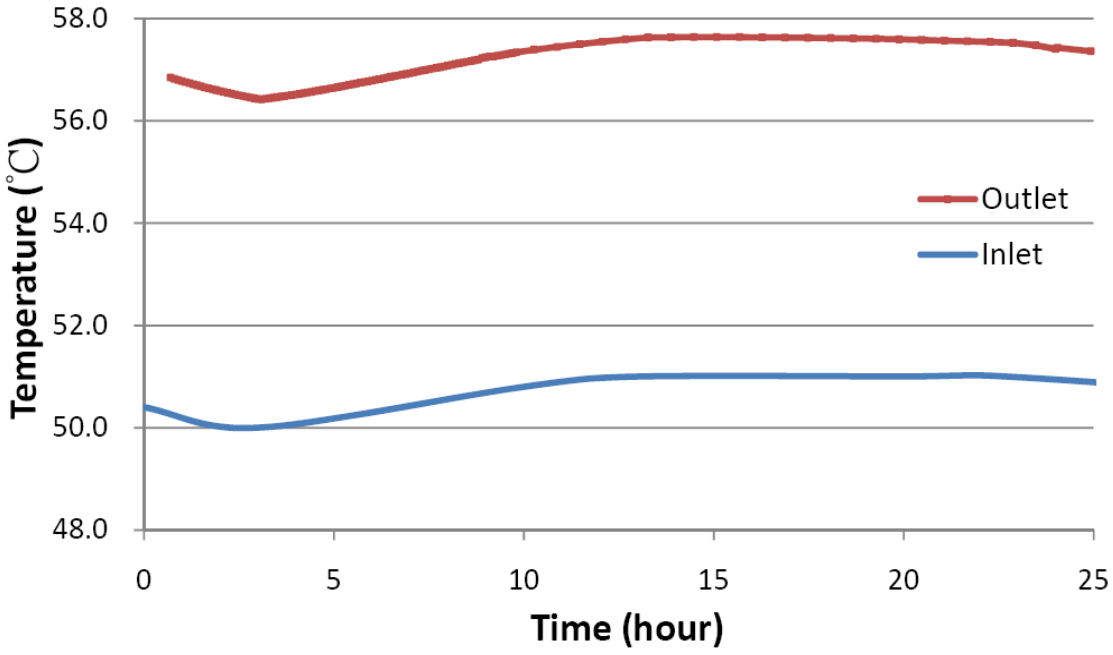


Figure 6-8. Cooling water inlet and outlet temperature for FLUENT

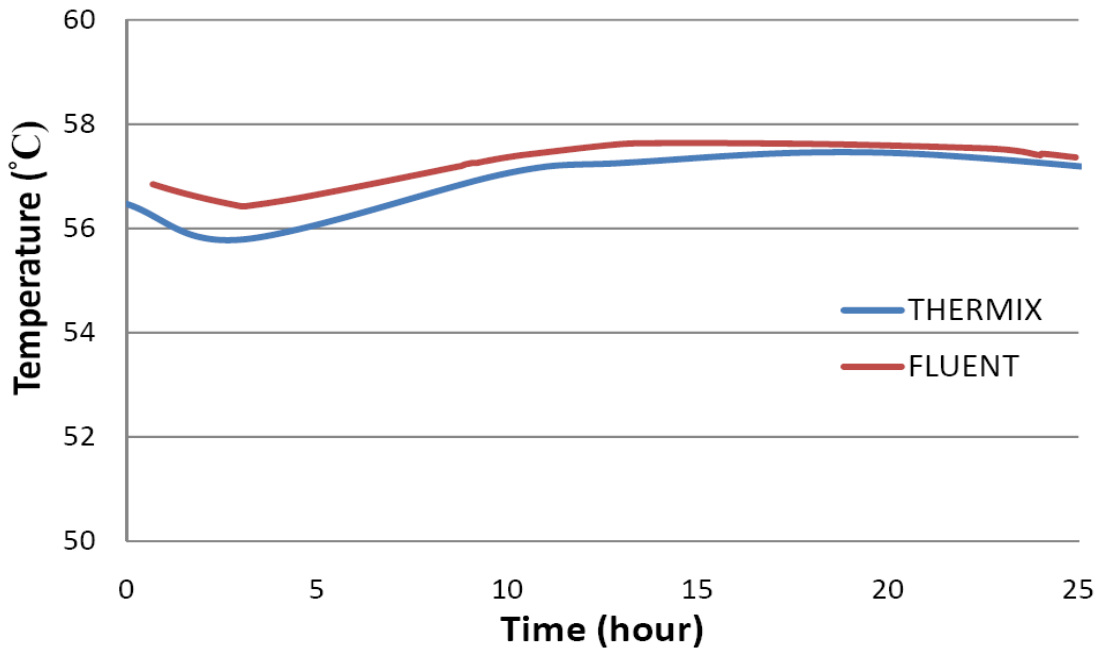


Figure 6-9. Cooling water outlet temperature from THERMIX and FLUENT

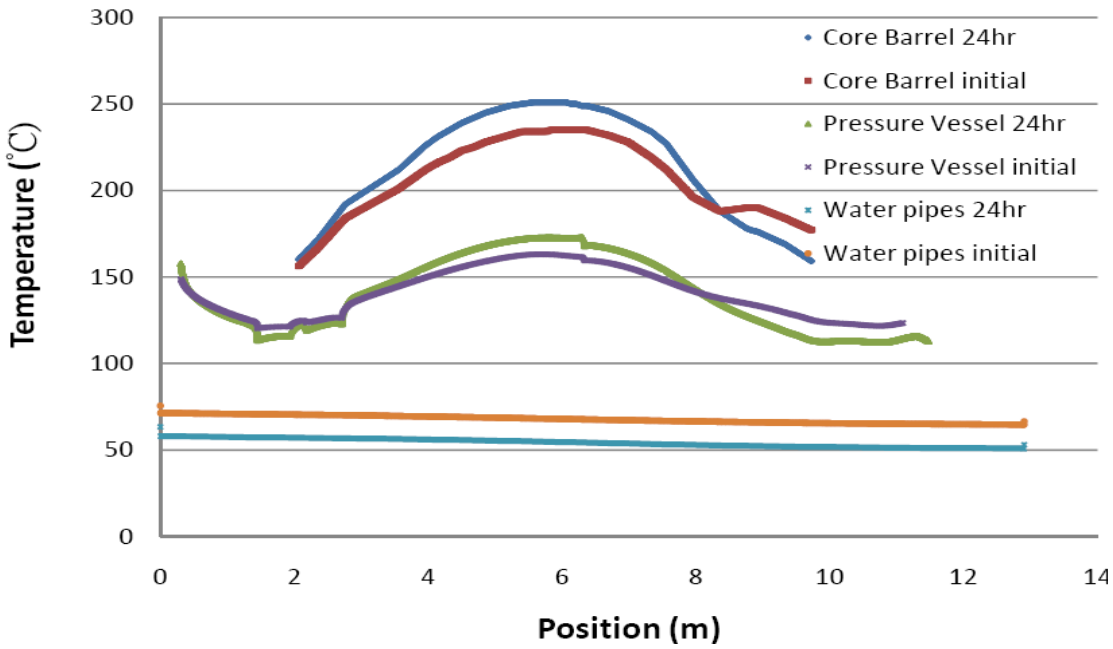


Figure 6-10. FLUENT temperature profiles:  initial and at 24 hours

Table 6-1. The results for new temperature profile in the heatup experiment (the second simulation in Model 1)

| Code | Max. Temperature of The pressure vessel | Max. Temperature of Water pipes | Temperature of water outlet |
|---|---|---|---|
| THERMIX | 331.0℃ | 80.9℃ | 74.4℃ |
| FLUENT | 302.2℃ | 85.0℃ | 80.0℃ |

Table 6-2. Different reproductions for the sensitivity studies

| Radiation | Turbulence | Density | Converged or not? |
|---|---|---|---|
| DO | k- ε | Boussinesq | Yes |
| P1 | k- ε | Boussinesq | No |
| S2S | k- ε | Boussinesq | No |
| DO | k- ε | Ideal Gas Law | Yes |
| DO | k- ω | Ideal Gas Law | Yes |
| DO | k- ω | Incompressible IGL | Yes |

Table 6-3. List of the sensitivity study and the corresponding models (DO means discrete ordinates)

| Trial | Solver | Mesh Size | Radiation | Turbulence | Density |
|---|---|---|---|---|---|
| 1 | Pressure based | 5mm | DO | k- ε | Boussinesq |
| 2 | Pressure based | 5mm | DO | k- ε | Ideal Gas Law |
| 3 | Pressure based | 5mm | DO | k- ω | Ideal Gas Law |
| 4 | Pressure based | 5mm | DO | k- ω | Incompressible IGL |
| 5 | Pressure based | 5mm | DO | Laminar | Ideal Gas Law |

Table 6-4. The results of trials in heatup exercise in Model 2 (F. means FLUENT code)

| Code | Max. Temp. of pressure vessel | Max. Temp. of water pipes | Temp. of water outlet | Heat transfer rate | Water Temp. difference | Models |
|---|---|---|---|---|---|---|
| THERMIX | 331.0℃ | 80.9℃ | 74.4℃ | 200 kW | 9.9℃ | - |
| F. Trial 1 | 298.9℃ | 78.5℃ | 78.5℃ | 360.027 kW | 14.0℃ | k- ε , Bous. |
| F. Trial 2 | 300.2℃ | 79.0℃ | 79.0℃ | 328.916 kW | 14.5℃ | k- ε , IGL |
| F. Trial 3 | 308.9℃ | 79.9℃ | 79.9℃ | 348.013 kW | 15.4℃ | k-ω , IGL |
| F. Trial 4 | 309.2℃ | 80.3℃ | 80.3℃ | 346.780 kW | 15.8℃ | k-ω , InIGL |
| F. Trial 5 | 304.1℃ | 87.9℃ | 76.5℃ | 305.184 kW | 12.0℃ | Laminar, IGL |
| F. 3D* | 471.55℃ | 158.9℃ | 64.6℃ | 2.181 kW | 0.10℃ | k-ω , InIGL |

Temp. refers to temperature and Bous. refers to Boussinesq

*the 3-D reproduction contained only one water cooling pipe and it had to be multiplied by 100

Table 6-5. The results of the LOHS accident at initial (t=0s)

| Code | Max. Temperature of Core barrel | Max. Temperature of The pressure vessel | Max. Temperature of Water pipes |
|---|---|---|---|
| THERMIX | 236.2℃ | 176.2℃ | 64.0℃ |
| FLUENT | 235.0℃ | 163.1℃ | 71.4℃ |

Table 6-6. The results of the LOHS Accident at 24hr (t=86400s)

| Code | Max. Temperature of Core barrel | Max. Temperature of The pressure vessel | Max. Temperature of Water pipes |
|---|---|---|---|
| THERMIX | 252.5℃ | 190.0℃ | 64.2℃ |
| FLUENT | 248.8℃ | 173.1℃ | 57.4℃ |

# CHAPTER 7
# CONCLUSIONS

Two changes were made in the HTR-10 RCCS grid from Model 1 to Model 2: the pipe's elbows were removed and the mesh size was reduced. The new grid was used in two FLUENT simulations using the k-ω model to account for turbulence and the ideal gas law to account for density variations. This differs from previous simulations that used the realizable k-ε model and the Boussinesq approximation. Still, the same discrepancy exists between the CRP-3 [1] simulations and the FLUENT reproductions; the FLUENT reproductions yield higher total heat transfer rates and temperature changes in the water cooling pipes. The discrepancy is even more pronounced when the Boussinesq approximation was used for turbulence modeling as in Model 1. Subsequently, more FLUENT reproductions were run with other turbulence, density, and radiation models. These simulations are used to test the sensitivity of the grid to different models, but it yielded results that were still not similar to those of the CRP-3. [1]

As mentioned by the values given in Table 6-4, the k-ω model presented higher heat transfer rate than the k-ε model by 5.5% difference. One can say that the k-ω model provided a higher dissipation rate, but because the difference is not large, it is difficult to say which method is more accurate. . There is no guarantee which viscosity model is better than the other. However, when the density model was changed, the k-ω model still predicted a higher transfer rate than the k-ε model (Table 6-4); hence, although the difference is not large, the k-ε model is suggested to be used in the simulation rather than the k-ω model. As described above, this in order to prevent the heat removal ability from being overestimated. .

Many discrepancies exist between the THERMIX and FLUENT simulations. For the heatup experiment, FLUENT predicts a higher temperature increase in the cooling water as it absorbs heat from the reactor. Strangely, the THERMIX simulation does not predict the highest

water temperature at the cooling wall outlet, but somewhere upstream. In both the heatup experiment and the LOHS depressurization accident, the FLUENT and THERMIX simulations gave different temperatures, although both predicted temperatures within a sensible range.

Although many comparisons can be drawn between the FLUENT and THERMIX simulations, a code-to-code benchmarking is not possible due to problems with TECDOC 1163 [1], from which all operational data and boundary conditions were obtained. One problem is that in the heatup experiment, the core barrel is said to have a higher temperature than in the initial state of the LOHS depressurization accident, even though the power in the heatup experiment is lower by a factor of 50. Also, there is a discrepancy in the same temperature data as presented in a table and a corresponding graph in TECDOC 1163. These contradictions make the data untrustworthy. Future study would require clarification of these factual conflicts, as well as additional documentation on the benchmark exercises. When the clarified documents are obtained, the 3D model can start being reliably simulated.

APPENDIX A
VALUES FOR ALL PARAMETERS USED IN THE HAND CALCULATIONS

Table A-1. Surface Area ($m^2$)

| | Core Barrel | Pressure Vessel | Water Wall | Discrete Water Pipes |
|---|---|---|---|---|
| Total | 117.141 | 162.91 | 213.494 | 47.04 |
| Top | 11.824 | 27.762 | | |
| Side | 93.493 | 107.388 | | |
| Bottom | 11.824 | 27.762 | | |

Table A-2. Case 1: Heatup with temperature from Table A.1 [1], include top and bottom of the core barrel, and water wall

| | Ra | ν | α | β | k | k-effect | Lc | Pr |
|---|---|---|---|---|---|---|---|---|
| Helium | 1307.8 | 290E-6 | 434E-6 | 0.001907 | 0.22 | 0.41518 | 0.0440 | 0.668 |
| Air | 2.0353E8 | 27.34E-6 | 39.68E-6 | 0.002452 | 0.0343 | 1.293 | 0.4137 | 0.689 |

Table A-3. Case 2: Heatup with temperature from Table A.1 [1], only side of the core barrel, and water wall

| | Ra | ν | α | β | k | k-effect | Lc | Pr |
|---|---|---|---|---|---|---|---|---|
| Helium | 1372.6 | 290E-6 | 434E-6 | 0.001915 | 0.22 | 0.42023 | 0.0440 | 0.668 |
| Air | 2.0227E8 | 27.04E-6 | 39.24E-6 | 0.002467 | 0.0342 | 1.2845 | 0.4137 | 0.690 |

Table A-4. Case 3: Heatup with temperature from Table A.1 [1], include top and bottom of the core barrel, and discrete pipes

| | Ra | ν | α | β | k | k-effect | Lc | Pr |
|---|---|---|---|---|---|---|---|---|
| Helium | 1047.6 | 290E-6 | 434E-6 | 0.001873 | 0.22 | 0.39278 | 0.0440 | 0.668 |
| Air | 2.1225E8 | 28.43E-6 | 41.30E-6 | 0.002400 | 0.0355 | 1.3307 | 0.4137 | 0.689 |

Table A-5. Case 4: Heatup with temperature from Table A.1 [1], only side of the core barrel, and discrete pipes

| | Ra | ν | α | β | k | k-effect | Lc | Pr |
|---|---|---|---|---|---|---|---|---|
| Helium | 1089.1 | 290E-6 | 434E-6 | 0.001878 | 0.22 | 0.39662 | 0.0440 | 0.668 |
| Air | 2.1179E8 | 28.23E-6 | 41.02E-6 | 0.002408 | 0.0349 | 1.3257 | 0.4137 | 0.689 |

Table A-6. Case 5: Heatup with temperature from Figure 3.36 [1], include top and bottom of the core barrel, and water wall

| | Ra | ν | α | β | k | k-effect | Lc | Pr |
|---|---|---|---|---|---|---|---|---|
| Helium | 1373 | 290E-6 | 434E-6 | 0.001842 | 0.22 | 0.42026 | 0.0440 | 0.668 |
| Air | 2.0623E8 | 28.23E-6 | 41.01E-6 | 0.002408 | 0.0355 | 1.3539 | 0.4137 | 0.689 |

Table A-7. Case 6: Heatup with temperature from Figure 3.36 [1], only side of the core barrel, and water wall

| | Ra | ν | α | β | k | k-effect | Lc | Pr |
|---|---|---|---|---|---|---|---|---|
| Helium | 1414.1 | 290E-6 | 434E-6 | 0.001847 | 0.22 | 0.42337 | 0.0440 | 0.668 |
| Air | 2.0577E8 | 28.04E-6 | 40.73E-6 | 0.002418 | 0.0348 | 1.3119 | 0.4137 | 0.689 |

Table A-8. Case 7: Heatup with temperature from Figure 3.36 [1], include top and bottom of the core barrel, and discrete pipes

| | Ra | ν | α | β | k | k-effect | Lc | Pr |
|---|---|---|---|---|---|---|---|---|
| Helium | 1106.1 | 290E-6 | 434E-6 | 0.001808 | 0.22 | 0.39815 | 0.0440 | 0.668 |
| Air | 2.1361E8 | 29.38E-6 | 42.72E-6 | 0.002354 | 0.0355 | 1.3539 | 0.4137 | 0.688 |

Table A-9. Case 8: Heatup with temperature from Figure 3.36 [1], only side of the core barrel, and discrete pipes

| | Ra | ν | α | β | k | k-effect | Lc | Pr |
|---|---|---|---|---|---|---|---|---|
| Helium | 1118.9 | 290E-6 | 434E-6 | 0.001810 | 0.22 | 0.3993 | 0.0440 | 0.668 |
| Air | 2.1357E8 | 29.32E-6 | 42.63E-6 | 0.002357 | 0.0355 | 1.3524 | 0.4137 | 0.688 |

Table A-10. Case 9: Heatup with temperature from LOHS [1], include top and bottom of the core barrel, and water wall

| | Ra | ν | α | β | k | k-effect | Lc | Pr |
|---|---|---|---|---|---|---|---|---|
| Helium | 1007.2 | 290E-6 | 434E-6 | 0.002209 | 0.22 | 0.38894 | 0.0440 | 0.668 |
| Air | 1.7296E8 | 23.92E-6 | 34.60E-6 | 0.002637 | 0.0323 | 1.1697 | 0.4137 | 0.692 |

Table A-11. Case 10: Heatup with temperature from LOHS [1], only side of the core barrel, and water wall

| | Ra | ν | α | β | k | k-effect | Lc | Pr |
|---|---|---|---|---|---|---|---|---|
| Helium | 1121.3 | 290E-6 | 434E-6 | 0.002227 | 0.22 | 0.39951 | 0.0440 | 0.668 |
| Air | 1.6553E8 | 23.47E-6 | 33.93E-6 | 0.002664 | 0.0321 | 1.1476 | 0.4137 | 0.692 |

Table A-12. Case 11: Heatup with temperature from LOHS [1], include top and bottom of the core barrel, and discrete water pipes

| | Ra | ν | α | β | k | k-effect | Lc | Pr |
|---|---|---|---|---|---|---|---|---|
| Helium | 802.54 | 290E-6 | 434E-6 | 0.002177 | 0.22 | 0.3675 | 0.0440 | 0.668 |
| Air | 1.8738E8 | 24.68E-6 | 35.73E-6 | 0.002594 | 0.0328 | 1.2097 | 0.4137 | 0.691 |

Table A-13. Case 12: Heatup with temperature from LOHS [1], only side of the core barrel, and discrete water pipes

| | Ra | ν | α | β | k | k-effect | Lc | Pr |
|---|---|---|---|---|---|---|---|---|
| Helium | 904.31 | 290E-6 | 434E-6 | 0.002193 | 0.22 | 0.3786 | 0.0440 | 0.668 |
| Air | 1.8191E8 | 24.28E-6 | 35.13E-6 | 0.002617 | 0.0326 | 1.1921 | 0.4137 | 0.691 |

# APPENDIX B
# CALCULATED VALUES FOR TOTAL DECAY HEAT

Table B-1. Decay heat calculations versus cooling time.

| Ptotal (kW) | Time (s) | Ptotal (kW) | Time (s) | Ptotal (kW) | Time (s) |
|---|---|---|---|---|---|
| 165.23 | 0.00001 | 31.38 | 1.2 | 24.44 | 10.5 |
| 110.67 | 0.0001 | 31.13 | 1.3 | 24.26 | 11 |
| 76.24 | 0.001 | 30.90 | 1.4 | 24.09 | 11.5 |
| 54.52 | 0.01 | 30.69 | 1.5 | 23.91 | 12 |
| 49.71 | 0.02 | 30.49 | 1.6 | 23.74 | 12.5 |
| 47.19 | 0.03 | 30.14 | 1.8 | 23.58 | 13 |
| 45.52 | 0.04 | 29.82 | 2 | 23.42 | 13.5 |
| 44.29 | 0.05 | 29.15 | 2.5 | 23.26 | 14 |
| 43.33 | 0.06 | 28.60 | 3 | 23.11 | 14.5 |
| 42.54 | 0.07 | 28.14 | 3.5 | 22.96 | 15 |
| 41.87 | 0.08 | 27.73 | 4 | 21.59 | 20 |
| 40.80 | 0.1 | 27.36 | 4.5 | 19.33 | 30 |
| 37.74 | 0.2 | 27.03 | 5 | 17.47 | 40 |
| 36.13 | 0.3 | 26.72 | 5.5 | 15.90 | 50 |
| 35.06 | 0.4 | 26.44 | 6 | 12.81 | 75 |
| 34.26 | 0.5 | 26.17 | 6.5 | 10.58 | 100 |
| 33.63 | 0.6 | 25.92 | 7 | 7.74 | 150 |
| 33.11 | 0.7 | 25.68 | 7.5 | 6.15 | 200 |
| 32.67 | 0.8 | 25.45 | 8 | 5.24 | 250 |
| 32.29 | 0.9 | 25.24 | 8.5 | 4.69 | 300 |
| 31.95 | 1 | 25.03 | 9 | 4.12 | 400 |
| 31.80 | 1.05 | 24.83 | 9.5 | 3.83 | 500 |
| 31.65 | 1.1 | 24.63 | 10 | | |

LIST OF REFERENCES


1. "Heat Transport and Afterheat Removal for Gas Cooled Reactors Under Accident Conditions", IAEA, CRP-3 TECDOC 1163, P.64-103, Austria, 2000.

2. Zuoyi Zhang, Zongxin Wu, Yuanhui Xu, Yuliang Sun, Fu Li, "Design of Chinese Modular High-Temperature Gas-Cooled Reactor HTR-PM." 2nd International Topic Meeting on HIGH TEMPERATURE REACTOR TECHNOLOGY, Beijing, China, Sep. 2004

3. F.M. Mitenkov, N. G. Kodochigov, A. V. Vasaev, V. F. Golovko, "High-Temperature Gas-Cooled Reactors-Energy Source For Industrial Production of Hydrogen." Atomic Energy, Vol. 97, No. 6, P. 829-840, 2004

4. FLUENT 6.3.26, Copyright 2006, Fluent Inc-Lebanon, NH

5. Zuying Gao, Shuyan He, and Min Zhang, "Afterheat Removal for HTR-10 Test Module Under Accident Conditions", Thermal-hydraulic Department of Institute of Nuclear Energy Technology, Tsinghua University, Beijing, China

6. Zuying Gao, Baoyan Lee, and Zhiqiang Jiang, "Benchmark Problem Definition of HTR-10", Thermal-hydraulic Department of Institute of Nuclear Energy Technology, Tsinghua University, Beijing, China, March 1997.

7. Zuying Gao, Lei Shi. "Thermal Hydraulic Calculation of The HTR-10 for The Initial and Equilibrium Core", Institute of Nuclear Energy Technology, Tsinghua University. Beijing, China. March 2002.

8. Anne Charmeau, "A Computational Thermal-Fluid Modeling Approach to Pulsed and Steady Gas Core Reactors." Master's Thesis, University of Florida, 2004

9. FLUENT 6.3 User's Guide, Fluent Inc., Lebanon, NH, 2006.

10. Suyuan Yu, Junjie Liu, Weidong Zuo, Shuysn He, "Sealing Behavior of The HTR-10 The Pressure Vessel Flanges," Institute of Nuclear Energy Technology, Tsinghua University. Beijing, China, 2002.

11. Zongxin Wu, Dengcai Lin, Daxin Zhong, "The Design Features of The HTR-10", Institute of Nuclear Energy and Technology, Tsinghua University, Beijing, China, March 2002.

12. "Fundamentals of Heat and Mass Transfer" Sixth Edition, Chapter 9, P.590-591, John Wiley&Sons(Asia) Pte Ltd, 2007

13. "Fundamentals of Heat and Mass Transfer" Sixth Edition, Chapter 13, P.832-833, John Wiley&Sons(Asia) Pte Ltd, 2007

14. Neil E. Todreas, Mujid S. Kazimi “Nuclear System I Thermal Hydraulic Fundamentals” , Chapter 3, P.66

15. Shouyin Hu, Ruipian Wang, “POWER OPERATION COMMISSIONING TESTS OF HTR-10”, 2nd International Topic Meeting on HIGH TEMPERATURE REACTOR TECHNOLOGY, Beijing, China, Sep. 2004

# BIOGRAPHICAL SKETCH

Hong-Chan Wei was born in 1982 in Kaohsiung city in Taiwan, and graduated from the Kaohsiung Senior High School in June 2000. He majored in physics at National Taiwan Normal University in Fall 2000, and obtained his diploma of Bachelor of Science in June 2004. After four years training in physics, he understood all fundamental physics and spent one following year teaching in the senior high school for contributing his knowledge. In 2007, he got the admission of Graduate School from University of Florida, and pursued a Master of Science Degree in the Nuclear and Radiological Engineering Department.